(Bartolo et al. 2001; Wands et al. 2002; Byrnes & Wands 2006). Thus we find a relation (Savelainen et al. 2013; Valiviita et al. 2012; Kawasaki & Sekiguchi 2008):

$$r = \left(1 - \cos^2\Delta\right)\tilde{r}, \tag{141}$$

i.e., the tensor-to-scalar ratio at the primordial time (r) is smaller than the ratio at the Hubble radius exit time ($\tilde{r}$).

The derivation of Eq. (141) assumes that the adiabatic and isocurvature perturbations are uncorrelated at Hubble radius exit ($\cos\tilde{\Delta} = 0$), and that all the possible primordial correlation ($\cos\Delta \neq 0$) appears from the evolution of super-Hubble perturbations between Hubble exit and the primordial time. This is true to leading order in the slow-roll parameters, but inflationary models that break slow roll might produce perturbations that are strongly correlated already at the Hubble radius exit time. In these cases the correlation would depend on the details of the particular model, such as the detailed shape of the potential and the interactions of the fields. However, a generic prediction of slow-roll inflation is that, at Hubble radius exit, the cross-correlation $\tilde{\mathcal{P}}_{\mathcal{R}I}$ is very weak, and indeed is of the order of the slow-roll parameters compared to the auto-correlations $\tilde{\mathcal{P}}_{\mathcal{R}\mathcal{R}}$ and $\tilde{\mathcal{P}}_{II}$ (see, e.g., Byrnes & Wands 2006). Thus, for slow-roll models, $|\cos\tilde{\Delta}| = O(\text{slow-roll parameters}) \ll 1$.

In our analysis, we fix the tensor spectral index by the leading-order inflationary consistency relation, which now reads (Wands et al. 2002)

$$n_{\rm t} = -\frac{\tilde{r}}{8} = -\frac{r}{8\left(1-\cos^2\Delta\right)}. \tag{142}$$

Assuming a uniform prior for r would lead to huge negative $n_{\rm t}$ whenever $\cos^2\Delta$ was close to one. Therefore, when studying the CDI+r case we assume a uniform prior on $\tilde{r}$ at $k = 0.05\,\mathrm{Mpc}^{-1}$ (for details, see Savelainen et al. 2013).

Surprisingly, allowing for a generally-correlated CDI mode (i.e., three extra parameters) hardly changes the constraints on r from those obtained in the pure adiabatic model. In Fig. 50 we demonstrate this in a "standard" plot of $r_{0.002}$ versus adiabatic spectral index.

From Table 16 we notice that, with *Planck* TT+lowP and TT, TE, EE+lowP, fixing r to 0.1 tightens constraints on the primordial isocurvature fraction at large scales. This is as we expected, since both tensor and isocurvature perturbations add power at low ℓ, and the data do not prefer this. However, the shapes of the tensor spectrum and correlation spectrum are such that negative correlation cannot efficiently cancel the unwanted extra power over all scales produced by tensor perturbations (at $\ell \lesssim 70$). Therefore, the correlation fraction $\cos\Delta$ is almost unaffected. However, when we allow r to vary, the cancelation mechanism works to some degree when using *Planck* TT+lowP data, leading to more negative $\cos\Delta$ than without r: with varying r we have $\cos\Delta$ in the range $(-0.43, 0.20)$, while without r it is in $(-0.30, 0.20)$, at 95% CL. As there is now some cancellation of power at large scales, the constraint on $\beta_{\rm iso}(k_{\rm low})$ weakens slightly from 0.041 without r to 0.043 with r. On the other hand, the high-ℓ polarization data constrain the correlation to be so close to zero that with *Planck* TT, TE, EE+lowP the results for $\cos\Delta$ with and without r are almost identical.

The mean value of $\cos\Delta$ in the CDI+r cases is -0.071 (TT+lowP) and -0.076 (TT, TE, EE+lowP). Therefore, $1 - \cos^2\Delta \approx 0.99$, and so we do not expect a large difference between the primordial r and the Hubble radius exit value $\tilde{r}$. The smallness of the difference is evident in Table 15. To summarize, CDI hardly affects the determination of r from the *Planck* data,

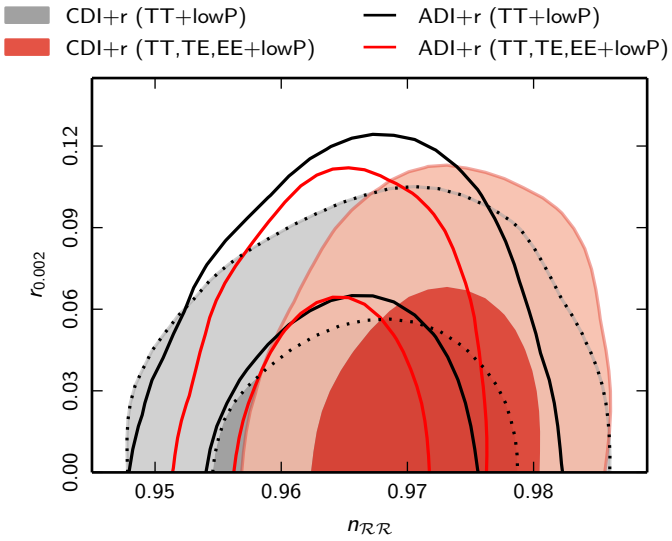

Fig. 50. 68% and 95% CL constraints on the primordial adiabatic spectral index $n_{\mathcal{R}\mathcal{R}}$ and the primordial tensor-to-scalar ratio r (more accurately, in the CDI+r model, the primordial tensor-to-curvature power ratio) at $k = 0.002\,\mathrm{Mpc}^{-1}$. Filled contours are for generally-correlated ADI+CDI and solid contours for the pure adiabatic model.

Table 15. 95% CL upper bounds on the tensor-to-scalar ratio (actually the tensor-to-curvature power ratio) at the primordial time, r, and earlier, at the Hubble radius exit time during inflation, $\tilde{r}$, at $k = 0.05\,\mathrm{Mpc}^{-1}$.

Model (and data)	$r_{0.05}$	$\tilde{r}_{0.05}$	$C_{10}^{\rm tens}/C_{10}^{\rm scal}$
CDI+r (TT+lowP)	0.086	0.089	0.041
ADI+r (TT+lowP)	0.101	0.101	0.048
CDI+r (TT, TE, EE+lowP)	0.092	0.092	0.043
ADI+r (TT, TE, EE+lowP)	0.094	0.094	0.044

Notes. In the pure adiabatic case r and $\tilde{r}$ are equal. In the last column $C_{10}^{\rm tens}/C_{10}^{\rm scal}$ indicates the tensor contribution to the temperature angular power at $\ell = 10$ relative to the temperature power from scalar perturbations ($C_{10}^{\rm scal} = C_{10}^{\mathcal{R}\mathcal{R}} + C_{10}^{\mathcal{R}I} + C_{10}^{I\mathcal{R}} + C_{10}^{II}$).

and allowing for tensor perturbations hardly affects the determination of the non-adiabaticity parameters.

11.5. Special CDI cases

Next we study three one-parameter CDI extensions to the adiabatic model. In all these extensions the isocurvature mode modifies only the largest angular scales, since we either fix n_{II} to unity ("axion") or to the adiabatic spectral index ("curvaton I/II"). As can be seen from Fig. 43, the polarization E mode at multipoles $\ell \gtrsim 200$ will not be significantly affected by this type of CDI mode. Therefore, these models are much less sensitive to residual systematic effects in the high-ℓ polarization data than the generally-correlated models.

11.5.1. Uncorrelated ADI+CDI ("Axion")

We start with an uncorrelated mixture of adiabatic and CDI modes ($\mathcal{P}_{\mathcal{R}I} = 0$) and make the additional assumption that $\mathcal{P}_{II}^{(2)} = \mathcal{P}_{II}^{(1)}$, i.e., we assume unit isocurvature spectral index, $n_{II} = 1$. Constraints in the $(n_{\mathcal{R}\mathcal{R}}, \beta_{\rm iso})$ plane are presented in

Table 16. Constraints on mixed adiabatic and isocurvature models.

Model (and data)	$100\beta_{\rm iso}(k_{\rm low})$	$100\beta_{\rm iso}(k_{\rm mid})$	$100\beta_{\rm iso}(k_{\rm high})$	$100\cos\Delta$	$100\alpha_{\mathcal{RR}}(2,2500)$	Δn	$\Delta\chi^2$	$\ln B$
General models:								
CDI (TT+lowP)	4.1	35.4	56.9	[−30:20]	[98.1:101.5]	3	−2.1	−8.8
CDI (TT+lowP+WP)	4.2	35.5	57.2	[−31:23]	[97.9:101.4]	3	−1.8	−9.1
CDI (TT, TE, EE+lowP)	2.0	[3.4:28.1]	[3.1:51.8]	[−6:20]	[98.5:99.9]	3	−5.3	−8.8
CDI (TT, TE, EE+lowP+WP)	2.1	[2.3:28.4]	[2.6:52.1]	[−7:21]	[98.5:99.9]	3	−5.5	−8.2
CDI (TT+lowP+lensing)	4.5	37.9	59.4	[−28:17]	[98.1:101.1]	3	−1.2	−8.8
NDI (TT+lowP)	14.3	22.4	27.4	[−33:1]	[98.6:104.0]	3	−2.0	−5.3
NDI (TT, TE, EE+lowP)	7.3	[3.4:19.3]	[3.5:26.7]	[−9:10]	[97.8:100.1]	3	−5.5	−5.5
NDI (TT+lowP+lensing)	15.8	[1.4:24.1]	[0.3:28.4]	[−32:0]	[98.6:104.0]	3	−2.8	−4.6
NVI (TT+lowP)	8.3	[0.1:10.2]	11.9	[−26:6]	[97.6:102.3]	3	−2.8	−6.3
NVI (TT, TE, EE+lowP)	7.4	[0.9:7.4]	[0.4:8.8]	[−22:−4]	[99.2:102.0]	3	−6.2	−6.5
NVI (TT+lowP+lensing)	9.7	[0.4:11.6]	13.1	[−23:7]	[97.1:102.0]	3	−2.5	−6.5
General models + r:								
CDI+r=0.1 (TT+lowP)	3.4	38.7	63.9	[−33:24]	[98.1:101.4]	3	−5.4	−8.9
CDI+r=0.1 (TT, TE, EE+lowP)	1.6	[4.4:31.7]	[6.9:59.2]	[−6:22]	[98.6:99.9]	3	−6.3	−8.1
CDI+r (TT+lowP)	4.3	34.9	56.2	[−43:20]	[97.9:102.4]	3	−3.3	−7.7
CDI+r (TT, TE, EE+lowP)	1.7	[3.9:29.0]	[5.8:53.8]	[−5:21]	[98.6:99.9]	3	−5.1	−7.2
Special CDI cases:								
Uncorrelated, $n_{\mathcal{II}} = 1$								
"axion" (TT+lowP)	3.3	3.7	3.8	0	[98.5:100]	1	0.0	−5.2
"axion" (TT, TE, EE+lowP)	3.5	3.8	3.9	0	[98.4:100]	1	−0.2	−4.9
"axion" (TT+lowP+lensing)	3.9	4.3	4.4	0	[98.3:100]	1	0.0	−5.0
Fully correlated, $n_{\mathcal{II}} = n_{\mathcal{RR}}$								
"curvaton I" (TT+lowP)	0.18	0.18	0.18	100	[97.5:100.0]	1	−0.1	−8.1
"curvaton I" (TT, TE, EE+lowP)	0.13	0.13	0.13	100	[97.8:99.9]	1	0.0	−7.8
"curvaton I" (TT+lowP+lensing)	0.22	0.22	0.22	100	[97.3:99.7]	1	0.0	−8.5
Fully anti-correlated, $n_{\mathcal{II}} = n_{\mathcal{RR}}$								
"curvaton II" (TT+lowP)	0.64	0.64	0.64	−100	[100.5:105.1]	1	−1.1	−5.4
"curvaton II" (TT, TE, EE+lowP)	0.08	0.08	0.08	−100	[100.1:101.8]	1	0.0	−8.9
"curvaton II" (TT+lowP+lensing)	0.52	0.52	0.52	−100	[100.4:104.4]	1	−0.6	−6.3

Notes. For each mixed model, we report 95% CL bounds on the fractional primordial contribution of isocurvature modes at three comoving wavenumbers ($k_{\rm low} = 0.002\,{\rm Mpc}^{-1}$, $k_{\rm mid} = 0.050\,{\rm Mpc}^{-1}$, and $k_{\rm high} = 0.100\,{\rm Mpc}^{-1}$), as well as the scale-independent primordial correlation fraction, $\cos\Delta$. The fractional adiabatic contribution to the observed temperature variance is denoted by $\alpha_{\mathcal{RR}}(2,2500)$, and from this the nonadiabatic contribution can be calculated as $\alpha_{\rm non\text{-}adi} = 1 - \alpha_{\mathcal{RR}}(2,2500)$. The number of extra parameters compared with the corresponding pure adiabatic model is denoted by Δn, and $\Delta\chi^2$ is the difference between the χ^2 of the best-fitting mixed and pure adiabatic models. (A negative $\Delta\chi^2$ means that the mixed model is a better fit to the data.) In the last column we give the difference between the logarithm of Bayesian evidences. (A negative $\ln B = \ln(P_{\rm ISO}/P_{\rm ADI})$ means that Bayesian model comparison disfavours the mixed model. With our settings of `MultiNest` the uncertainty in these numbers is about ±0.5.)

Fig. 51. This model is the only case for which our new results do not improve over bounds from PCI13. At $k_{\rm mid} = 0.050\,{\rm Mpc}^{-1}$, we find $\beta_{\rm iso} < 0.038$ (95% CL, TT, TE, EE+lowP; see Table 16), compared with $\beta_{\rm iso} < 0.039$ using *Planck* 2013 and low-ℓ WMAP data. This is not surprising, since fixing $n_{\mathcal{II}}$ to unity implies that bounds are dominated by measurements on very large angular scales, $\ell \lesssim 30$, as can easily be understood from Fig. 43. Hence the results are insensitive to the addition of better high-ℓ temperature data, or new high-ℓ polarization data.

We summarized in PCI13 why an uncorrelated CDI mode with $n_{\mathcal{II}} \approx 1$ can be produced in axion models under a number of restrictive assumptions: the Peccei-Quinn symmetry should be broken before inflation; it should not be restored by quantum fluctuations of the inflaton or by thermal fluctuations when the Universe reheats; and axions produced through the misalignment angle should contribute to a sizable fraction (or all) of the dark matter. Under all of these assumptions, limits on $\beta_{\rm iso}$ can be used to infer a bound on the energy scale of inflation, using Eq. (73) of PCI13. This bound is strongest when all the dark matter is assumed to be in the form of axions. In that case, the limit on $\beta_{\rm iso}(k_{\rm mid})$ for *Planck* TT, TE, EE+lowP gives

$$H_{\rm inf} < 0.86\times10^{7}\,{\rm GeV}\left(\frac{f_a}{10^{11}\,{\rm GeV}}\right)^{0.408} \quad (95\%\ {\rm CL}), \qquad (143)$$

where $H_{\rm inf}$ is the expansion rate at Hubble radius exit of the scale corresponding to $k_{\rm mid} = 0.050\,{\rm Mpc}^{-1}$ and f_a is the Peccei-Quinn symmetry-breaking energy scale.

11.5.2. Fully correlated ADI+CDI ("Curvaton I")

Another interesting special case of mixed adiabatic and CDI (or BDI) perturbations is a model where these perturbations are primordially fully correlated and their power spectra have the same shape. These cases are obtained by setting $\mathcal{P}^{(1)}_{\mathcal{RI}} = (\mathcal{P}^{(1)}_{\mathcal{RR}}\mathcal{P}^{(1)}_{\mathcal{II}})^{1/2}$,

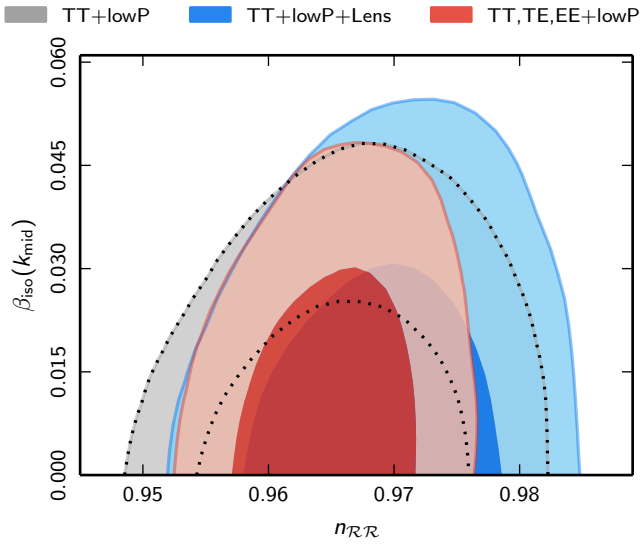

Fig. 51. Uncorrelated ADI+CDI with $n_{\mathcal{II}} = 1$ ("axion").

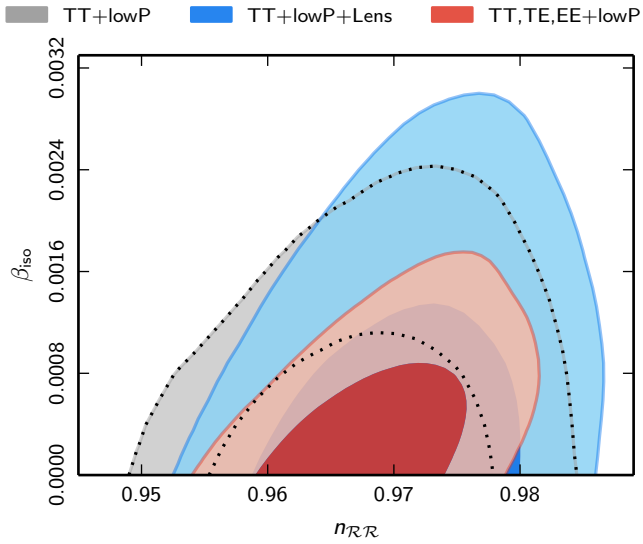

Fig. 52. Fully correlated ADI+CDI with $n_{\mathcal{II}} = n_{\mathcal{RR}}$ ("curvaton I"). Since the spectral indices are equal, the primordial isocurvature fraction $\beta_{\rm iso}$ is scale-independent.

which, by condition (136), implies that the corresponding statement holds at scale k_2 and indeed at any scale. In addition, we set $\mathcal{P}^{(2)}_{\mathcal{II}} = (\mathcal{P}^{(2)}_{\mathcal{RR}}/\mathcal{P}^{(1)}_{\mathcal{RR}})\mathcal{P}^{(1)}_{\mathcal{II}}$, i.e., $n_{\mathcal{II}} = n_{\mathcal{RR}}$. From this it follows that $\beta_{\rm iso}$ is scale-independent. Therefore, this model has only one primary non-adiabaticity parameter, $\mathcal{P}^{(1)}_{\mathcal{II}}$.

A physically motivated example of this type of model is the curvaton model (Mollerach 1990; Linde & Mukhanov 1997; Enqvist & Sloth 2002; Moroi & Takahashi 2001; Lyth & Wands 2002; Lyth et al. 2003) with the following assumptions. (1) The average curvaton field value $\bar{\chi}_*$ is sufficiently below the Planck mass when cosmologically interesting scales exit the Hubble radius during inflation. (2) At Hubble radius exit, the curvature perturbation from the inflaton is negligible compared to the perturbation caused by the curvaton. (3) The same is true for any inflaton decay products after reheating. This means that, after reheating, the Universe is homogeneous, except for the spatially varying entropy (i.e., isocurvature perturbation) due to the curvaton field perturbations. (4) Later, CDM is created from the curvaton decay and baryon number after curvaton decay. This corresponds to case 4 presented in Gordon & Lewis (2003). (5) The curvaton contributes a significant amount to the energy density of the Universe at the time of the curvaton's decay to CDM, i.e., the curvaton decays late enough. (6) The energy density of curvaton particles possibly produced during reheating should be sufficiently low (Bartolo & Liddle 2002; Linde & Mukhanov 2006). (7) The small-scale variance of curvaton perturbations, $\Delta^2_s = \langle \delta\chi^2 \rangle_s / \bar{\chi}^2$, is negligible, so that it does not significantly contribute to the average energy density on CMB scales; see Eq. (102) in Sasaki et al. (2006). The last two conditions are necessary in order to have an almost-Gaussian curvature perturbation, as required by the *Planck* observations. Indeed, if they are not valid, a large $f^{\rm local}_{\rm NL}$ follows, as discussed below. The conditions (6) and (7) are related, since curvaton particles would add a homogeneous component to the average energy density on large scales, and hence we can describe their effect by $\Delta^2_s = \rho_{\chi,\,\rm particles}/\rho_{\bar{\chi},\,\rm field}$, where $\rho_{\bar{\chi},\,\rm field}$ is the average energy density of the classical curvaton field on large scales; see Eq. (98) in Sasaki et al. (2006). Then the total energy density carried by the curvaton will be $\bar{\rho}_\chi = \rho_{\bar{\chi},\,\rm field} + \rho_{\chi,\,\rm particles}$.

The amount of isocurvature and non-Gaussianity present after curvaton decay depends on the "curvaton decay fraction"

$$r_{\rm D} = \frac{3\bar{\rho}_\chi}{3\bar{\rho}_\chi + 4\bar{\rho}_{\rm radiation}} \tag{144}$$

evaluated at curvaton decay time. If conditions (6) and (7) do not hold, then the isocurvature perturbation disappears.[22]

The curvaton scenario presented here is one of the simplest to test against observations. It should be noted that at least the conditions (1)–(5) listed at the beginning of this subsection should be satisfied simultaneously. Indeed, if we relax some of these conditions, almost any type of correlation can be produced. For example, the relative correlation fraction can be written as $\cos\Delta = \sqrt{\lambda/(1+\lambda)}$, where $\lambda = (8/9) r_{\rm D}^2 \epsilon_* (M_{\rm Pl}/\bar{\chi}_*)^2$. Therefore, the model is fully correlated only if $\lambda \gg 1$. If the slow-roll parameter ϵ_* is very close to zero or the curvaton field value $\bar{\chi}_*$ is large compared to the Planck mass, this model leads to almost uncorrelated perturbations.

As seen in Fig. 52 and Table 16, the upper bound on the primordial isocurvature fraction in the fully-correlated ADI+CDI model weakens slightly when we add the *Planck* lensing data to *Planck* TT+lowP, whereas adding high-ℓ TE, EE tightens the upper bound moderately. With all of these three data combinations, the pure adiabatic model gives an equally good best-fit χ^2 as the fully-correlated ADI+CDI model. Bayesian model comparison strengthens the conclusion that the data disfavour this model with respect to the pure adiabatic model.

The isocurvature fraction is connected to the curvaton decay fraction in Eq. (144) by

$$\beta_{\rm iso} \approx \frac{9(1-r_{\rm D})^2}{r_{\rm D}^2 + 9(1-r_{\rm D})^2} \tag{145}$$

(see case 4 in Gordon & Lewis 2003). We can convert the constraints on $\beta_{\rm iso}$ from Table 16 into constraints on $r_{\rm D}$ and further

[22] Indeed, if curvaton particles are produced during reheating, they can be expected to survive and outweigh other particles at the moment of curvaton decay, but by how much depends on the details of the model. As the curvaton field (during its oscillations) and the curvaton particles have the same equation of state and they decay simultaneously, no isocurvature perturbations are produced.

into the non-Gaussianity parameter assuming a quadratic potential for the curvaton and instantaneous decay[23] (Sasaki et al. 2006):

$$f_{\rm NL}^{\rm local} = \left(1+\Delta_s^2\right)\frac{5}{4r_{\rm D}} - \frac{5}{3} - \frac{5r_{\rm D}}{6}. \quad (146)$$

If conditions (6) and (7) hold, i.e., $\Delta_s^2 = 0$, as implicitly assumed, e.g., in Bartolo et al. (2004a,b), then the smallest possible value of $f_{\rm NL}^{\rm local}$ is $-5/4$, which is obtained when $r_{\rm D} = 1$, and Eqs. (145) and (146) yield for the various *Planck* data sets (at 95% CL):[24]

$$\text{TT+lowP:}\quad \beta_{\rm iso} < 0.0018 \Rightarrow 0.9860 < r_{\rm D} \le 1 \Rightarrow -1.250 \le f_{\rm NL}^{\rm local} < -1.220, \quad (147)$$

$$\text{TT+lowP+lensing:}\quad \beta_{\rm iso} < 0.0022 \Rightarrow 0.9845 < r_{\rm D} \le 1 \Rightarrow -1.250 \le f_{\rm NL}^{\rm local} < -1.217, \quad (148)$$

$$\text{TT, TE, EE+lowP:}\quad \beta_{\rm iso} < 0.0013 \Rightarrow 0.9882 < r_{\rm D} \le 1 \Rightarrow -1.250 \le f_{\rm NL}^{\rm local} < -1.225. \quad (149)$$

Thus the results for the simplest curvaton model remain unchanged from those presented in PCI13. In order to produce almost purely adiabatic perturbations, the curvaton should decay when it dominates the energy density of the Universe ($r_{\rm D} > 0.98$), and the non-Gaussianity parameter is constrained to close to its smallest possible value ($-5/4 < f_{\rm NL}^{\rm local} < -1.21$), which is consistent with the result $f_{\rm NL}^{\rm local} = 2.5 \pm 5.7$ (68% CL, from T only) found in Planck Collaboration XVII (2016).

11.5.3. Fully anticorrelated ADI+CDI ("Curvaton II")

The curvaton scenario or some other mechanism could also produce 100% anticorrelated perturbations, with $n_{II} = n_{\mathcal{RR}}$. The constraints in the $(n_{\mathcal{RR}}, \beta_{\rm iso})$ plane are presented in Fig. 53. Examples of this kind of model are provided by cases 2, 3, and 6 in Gordon & Lewis (2003). These lead to a fixed, large amount of isocurvature, e.g., in case 2 to $\beta_{\rm iso} = 9/10$, and are hence excluded by the data at very high significance. However, case 9 in Gordon & Lewis (2003), with a suitable $r_{\rm D}$ (i.e., $r_{\rm D} > R_{\rm c}$, where $R_{\rm c} = \rho_{\rm c}/(\rho_{\rm c}+\rho_{\rm b})$), leads to fully-anticorrelated perturbations and might provide a good fit to the data. In this case CDM is produced by curvaton decay while baryons are created earlier from inflaton decay products and do not carry a curvature perturbation. We obtain a very similar expression to Eq. (145), namely

$$\beta_{\rm iso} \approx \frac{9(1-r_{\rm D}/R_{\rm c})^2}{r_{\rm D}^2 + 9(1-r_{\rm D}/R_{\rm c})^2}. \quad (150)$$

[23] The formula $f_{\rm NL}^{\rm local} = 5/(4r_{\rm D})$ is often quoted or utilized, particularly in the older curvaton literature. This result, which follows from considering only squares of first order perturbations, is valid when $r_{\rm D}$ is close to zero (i.e., when $f_{\rm NL}^{\rm local}$ is very large). However, when $r_{\rm D}$ is close to unity or $f_{\rm NL}^{\rm local} \lesssim 10$, which is the case with the *Planck* measurements, the second and third terms of Eq. (146) are crucial. These follow from second order perturbation theory calculations. Coincidentally, if one erroneously uses the expression $5/(4r_{\rm D})$ in the limit $r_{\rm D} \to 1$, one obtains the result $+5/4$, whereas the correct formula (146) with $\Delta_s^2 = 0$ leads to $-5/4$ when $r_{\rm D} \to 1$.

[24] However, if Δ_s^2 was non-negligible, then all the constraints on $f_{\rm NL}^{\rm local}$ would shift upward. For example, with $\Delta_s^2 = 1$, our constraints on $\beta_{\rm iso}$ would translate to $0 \le f_{\rm NL}^{\rm local} \lesssim 0.03$. On the other hand, the *Planck* constraint of $f_{\rm NL}^{\rm local}$ can be converted to an upper bound $\Delta_s^2 = \rho_{\chi,\,\rm particles}/\rho_{\tilde{\chi},\,\rm field} < 8.5$ (95% CL from T only) as shown in Planck Collaboration XVII (2016).

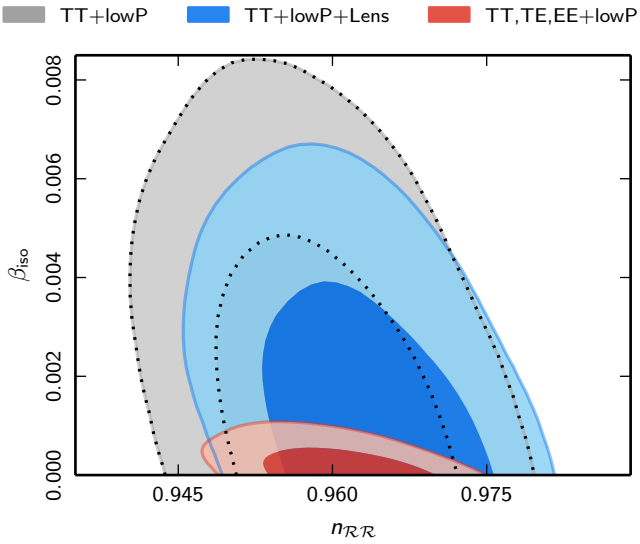

Fig. 53. Fully anticorrelated ADI+CDI with $n_{II} = n_{\mathcal{RR}}$ ("curvaton II").

We convert this to an approximate constraint on $r_{\rm D}$ by fixing $R_{\rm c}$ to its best-fit value, $R_{\rm c} = 0.8437$ (*Planck* TT+lowP), within this model. The results for the various *Planck* data sets are:

$$\text{TT+lowP: } \beta_{\rm iso} < 0.0064 \Rightarrow 0.8437 < r_{\rm D} < 0.8632 \Rightarrow -0.9379 < f_{\rm NL}^{\rm local} < -0.8882, \quad (151)$$

$$\text{TT+lowP+lensing: } \beta_{\rm iso} < 0.0052 \Rightarrow 0.8437 < r_{\rm D} < 0.8612 \Rightarrow -0.9329 < f_{\rm NL}^{\rm local} < -0.8882, \quad (152)$$

$$\text{TT, TE, EE+lowP: } \beta_{\rm iso} < 0.0008 \Rightarrow 0.8437 < r_{\rm D} < 0.8505 \Rightarrow -0.9056 < f_{\rm NL}^{\rm local} < -0.8882. \quad (153)$$

After all the tests conducted in this section, both for the generally-correlated CDI, NDI, and NVI cases as well as for the special CDI cases, we conclude that within the spatially flat base ΛCDM model, the initial conditions of perturbations are consistent with the hypothesis of pure adiabaticity, a conclusion that is also supported by the Bayesian model comparison. Moreover, Planck Collaboration XVII (2016) reports a null detection of *isocurvature non-Gaussianity*, with polarization improving constraints significantly.

12. Statistical anisotropy and inflation

A key prediction of standard inflation, which in the present context includes all single field models of inflation as well as many multi-field models, is that the stochastic process generating the primordial cosmological perturbations is completely characterized by its power spectrum, constrained by statistical isotropy to depend only on the multipole number ℓ. This statement applies at least to the accuracy that can be probed using the CMB given the limitations imposed by cosmic variance, since all models exhibit *some* level of non-Gaussianity. Nevertheless, more general Gaussian stochastic processes can be envisaged for which one or more special directions on the sky are singled out, so that the expectation values for the temperature multipoles take the form

$$\left\langle a_{\ell m}^T \left(a_{\ell' m'}^T\right)^* \right\rangle = C_{\ell m;\ell' m'}^{\rm TT}, \quad (154)$$

rather than the very special form

$$\left\langle a_{\ell m}^T \left(a_{\ell' m'}^T\right)^* \right\rangle = C_{\ell}^{\rm TT}\, \delta_{\ell,\ell'}\, \delta_{m,m'}, \quad (155)$$

which is the only possibility consistent with statistical isotropy.

The most general form for a Gaussian stochastic process on the sphere violating the hypothesis of statistical isotropy in Eq. (154) is too broad to be useful, given that we have only one sky to analyse. For $\ell < \ell_{\rm max}$, there are $O(\ell_{\rm max}^2)$ multipole expansion coefficients, compared with $O(\ell_{\rm max}^4)$ model parameters. Therefore, in order to make some progress on testing the hypothesis of statistical isotropy, we must restrict ourselves to examining only the simplest models violating statistical isotropy, for which the available data can establish meaningful constraints and for which one can hope to find a simple theoretical motivation.

12.1. Asymmetry: observations versus model building

In one simple class of statistically anisotropic models, we start with a map produced by a process respecting statistical isotropy, which becomes modulated by another field in the following manner to produce the observed sky map:

$$\delta T_{\rm sky}(\hat{\mathbf{\Omega}}) = \left(1 + M(\hat{\mathbf{\Omega}})\right) \delta T_{\rm s\text{-}i}(\hat{\mathbf{\Omega}}), \tag{156}$$

where $\hat{\mathbf{\Omega}}$ denotes a position on the celestial sphere and $\delta T_{\rm s\text{-}i}(\hat{\mathbf{\Omega}})$ is the outcome of the underlying statistically isotropic process before modulation. Roughly speaking, where the modulating field $M(\hat{\mathbf{\Omega}})$ is positive, power on scales smaller than the scale of variation of $M(\hat{\mathbf{\Omega}})$ is enhanced, whereas where $M(\hat{\mathbf{\Omega}})$ is negative, power is suppressed. We refer to this as a "power asymmetry." If $M(\hat{\mathbf{\Omega}}) = A\hat{\boldsymbol{d}} \cdot \hat{\mathbf{\Omega}}$, we have a model of dipolar modulation with amplitude A and direction $\hat{\boldsymbol{d}}$, but higher-order or mixed modulation may also be considered, such as a quadrupole modulation or modulation by a scale-invariant field $M(\hat{\mathbf{\Omega}})$, to name just a few special cases. Alternatively, and more closely tied to physical models, we can consider modulations of the position- or k-space fluctuations.

In Planck Collaboration XXIII (2014) and Planck Collaboration XVI (2016), the details of constructing efficient estimators for statistical anisotropy, in particular in the presence of realistic data involving sky cuts and possibly incompletely removed foreground contamination, are considered in depth. In addition, the question of the statistical significance of any detected "anomalies" from the expectations of base ΛCDM is examined in detail. Importantly, in the *absence* of a particular inflationary model for such an observed anomaly, the significance should be corrected for the "multiplicity of tests" that *could* have resulted in similarly-significant detections (i.e., for the "look elsewhere effect"), although applying such corrections can be ambiguous. In this paper, however, we consider only forms of statistical anisotropy that are predicted by specific inflationary models, and hence such corrections will not be necessary.

Several important questions can be posed regarding the link between statistical isotropy and inflation. In particular, we can ask the following questions. (1) Does a statistically significant finding of a violation of statistical isotropy falsify inflation? (2) If not, what sort of non-standard inflation could produce the required departure from statistical isotropy? (3) What other perhaps non-inflationary models could also account for the violation of statistical isotropy? In this section, we begin to address these questions by assessing the viability of an inflationary model for dipolar asymmetry, as well as by placing new limits on the presence of quadrupolar power asymmetry.

For the case of the observed dipolar asymmetry examined in detail in Planck Collaboration XVI (2016), there are two aspects that make inflationary model building difficult. First is the problem of obtaining a significant amplitude of dipole modulation. In Planck Collaboration XVI (2016) the asymmetry was found to have amplitude $A \approx 6$–7% on scales $2 \le \ell \le 64$. This compares with the expected value of $A = 2.9\%$ on these scales due to cosmic variance in statistically isotropic skies. One basic strategy for incorporating the violation of statistical isotropy into inflation is to consider some form of multi-field inflation and use one of the directions orthogonal to the direction of slow roll as the field responsible for the modulation. Obtaining the required modulation is problematic because most extra fields in multi-field inflation become disordered in a nearly scale-invariant way, just like the fluctuations in the field parallel to the direction of slow roll. What is needed resembles a pure gradient with no fluctuations of shorter wavelength. In Liddle & Cortês (2013) it was proposed that such a field could be produced using the supercurvature mode of open inflation. (See however the discussion in Kanno et al. 2013.) Also, in order to respect the $f_{\rm NL}$ constraints, one must avoid that the modulating field leave a direct imprint on the temperature anisotropy.

The second aspect which makes model building difficult for dipolar asymmetry is that the measured amplitude is strongly scale dependent, and on scales $\ell \gtrsim 100$ no significant detection of a dipolar modulation amplitude is made (Planck Collaboration XVI 2016), once our proper motion has been taken into account (Planck Collaboration XXVII 2014). On the other hand, the simplest models are scale-free and produce statistical anisotropy of the type described by the ansatz in Eq. (156), for which the bulk of the statistical weight should be detected at the resolution of the survey. To resolve this difficulty, Erickcek et al. (2009) proposed modulating CDI fluctuations generated within the framework of a curvaton scenario, because, unlike adiabatic perturbations, CDI perturbations entering the Hubble radius before last scattering contribute negligibly to the CMB fluctuations (recall Fig. 43).

The situation for the quadrupolar power asymmetry is different from the dipolar case in that no detection is currently claimed. Model building is easier than the dipolar case since no pure gradient modes are required, but also more difficult in that anisotropy during inflation is needed. While the isotropy of the recent expansion of the Universe (i.e., since the CMB fluctuations were first imprinted) is tightly constrained, bounds on a possible anisotropic expansion at early times are much weaker. Ackerman et al. (2007) proposed using constraints on the quadrupolar statistical anisotropy of the CMB to probe the isotropy of the expansion during inflation – that is, during the epoch when the perturbations now seen in the CMB first exited the Hubble radius. Assuming an anisotropic expansion during inflation, Ackerman et al. (2007) computed its impact on the three-dimensional power spectrum on super-Hubble scales by integrating the mode functions for the perturbations during inflation and beyond. Several sources of such anisotropy have been proposed, such as vector fields during inflation (Dimastrogiovanni et al. 2010; Soda 2012; Maleknejad et al. 2013; Schmidt & Hui 2013; Bartolo et al. 2013; Naruko et al. 2015), or an inflating solid or elastic medium (Bartolo et al. 2013).

12.2. Scale-dependent modulation and idealized estimators

The ansatz in Eq. (156) expressed in angular space may be rewritten in terms of the multipole expansion and generalized to include scale-dependent modulation by means of Wigner $3j$ symbols:

$$\left\langle a^T_{\ell m}\, a^T_{\ell' m'} \right\rangle = \sum_{L=0}^{\infty} \sum_{M=-L}^{+L} C^{\rm TT}_{\ell;\ell';L,M} \begin{pmatrix} \ell & \ell' & L \\ m & m' & M \end{pmatrix}. \tag{157}$$

Because of the symmetry of the left-hand side, the coefficients $C^{\rm TT}_{\ell;\ell';L,M}$ acquire a phase $(-1)^{\ell+\ell'+L}$ under interchange of ℓ and ℓ'. This is the most general form consistent with the hypothesis of Gaussianity. The usual isotropic power spectrum, which is the generic prediction of simple models of inflation, includes only the $L = 0$ term, where $C^{\rm TT}_{\ell;\ell';0,0} = C^{\rm TT}_\ell$ and the Wigner $3j$ symbol provides the $\delta_{\ell,\ell'}\delta_{m,m'}$ factor. The coefficients $C^{\rm TT}_{\ell;\ell';L,M}$ with $L > 0$ introduce statistical anisotropy.

If we assume that there is a common vector (corresponding to $L = 1$ on the celestial sphere) that defines the direction of the anisotropy of the power spectrum for all the terms of $L = 1$, we may adopt a more restricted ansatz for the bipolar modulation, so that

$$C^{\rm TT}_{\ell;\ell';1,M} = C^1_{\ell,\ell'} X^{(1)}_M, \tag{158}$$

where we assume that X_M is normalized (i.e., $\sum_M X_M X_M{}^* = 1$). In such a model, supposing that $C^1_{\ell,\ell'}$ is theoretically determined, but the orientation of the unit vector X_M is random and isotropically distributed on the celestial sphere, we may construct the following quadratic estimator for the direction:

$$X^{(L)}_M = \sum_{\ell,m}\sum_{\ell',m'} \frac{w_{\ell,\ell';L}}{(2L+1)(C_\ell)^{1/2}\,(C_{\ell'})^{1/2}} \times \begin{pmatrix} \ell & \ell' & L \\ m & m' & M \end{pmatrix} a^T_{\ell m}\, a^T_{\ell' m'}, \tag{159}$$

where the weights for the unbiased minimum variance estimator are given by

$$w_{\ell,\ell';L} = C^L_{\ell,\ell'} \left(\sum_{\ell,\ell'} C^L_{\ell,\ell'} \right)^{-1}. \tag{160}$$

This construction, which for the $L = 1$ case may be found in Moss et al. (2011) and Planck Collaboration XVI (2016), may be readily generalized to $L > 1$ in the above way.

12.3. Constraining inflationary models for dipolar asymmetry

In this section, we confront with *Planck* data the modulated curvaton model of Erickcek et al. (2009), which attempts to explain the observed large-scale power asymmetry via a gradient in the background curvaton field. In this model, the curvaton decays after CDM freeze out, which results in a nearly-scale-invariant isocurvature component between CDM and radiation. In the viable version of this scenario, the curvaton contributes negligibly to the CDM density. A long-wavelength fluctuation in the curvaton field initial value σ_* is assumed, with amplitude $\Delta\sigma_*$ across our observable volume. This modulates the curvaton isocurvature fluctuations according to $S_{\sigma\gamma} \approx 2\delta\sigma_*/\sigma_*$. The curvaton produces all of the final CDI fluctuations, which are nearly scale invariant, as well as a component of the final adiabatic fluctuations. Hence both of these components will be modulated, and the parameter space of the model will be constrained by observations of the power asymmetry on large and small scales, as well as the full-sky CDI fraction. In practice, the very tight constraints on small scale power asymmetry obtained in Planck Collaboration XVI (2016) imply a small curvaton adiabatic component, which implies that the CDI and adiabatic fluctuations are only weakly correlated. This model easily satisfies constraints due to the CMB dipole, quadrupole, and non-Gaussianity (Erickcek et al. 2009).

There are two main parameters that we constrain for this model. First, the fraction of adiabatic fluctuations due to the curvaton ξ is defined as

$$\xi \equiv \frac{\Sigma^2_\sigma \mathcal{P}_\sigma}{\mathcal{P}_{\mathcal{R}_{\rm inf}} + \Sigma^2_\sigma \mathcal{P}_\sigma}. \tag{161}$$

Here, $\mathcal{P}_{\mathcal{R}_{\rm inf}}$ and $\mathcal{P}_\sigma$ are the inflaton and curvaton primordial power spectra, respectively, and Σ_σ is the coupling from curvaton isocurvature to adiabatic fluctuations. (Up to a sign, ξ is equal to the correlation parameter.) Next, the coupling of curvaton to CDI, $M_{{\rm CDI}\sigma}$, is determined by the constant $\kappa \equiv M_{{\rm CDI}\sigma}/R \gtrsim -1$, where

$$R \equiv \frac{3\Omega_\sigma}{4\Omega_\gamma + 3\Omega_\sigma + 3\Omega_{\rm CDM}} \tag{162}$$

and all density parameters are evaluated just prior to curvaton decay. The isocurvature fraction can be written in terms of these two parameters by

$$\beta_{\rm iso} = \frac{9\kappa^2\xi}{1 + 9\kappa^2\xi}. \tag{163}$$

These parameters determine the modulation of the CMB temperature fluctuations via $\Delta C_\ell/C_\ell = 2K_\ell \Delta\sigma_*/\sigma_*$, where (Erickcek et al. 2009)

$$K_\ell \equiv \xi \frac{C^{\rm ad}_\ell + 9\kappa^2 C^{\rm iso}_\ell + 3\kappa C^{\rm cor}_\ell}{C^{\rm ad}_\ell + \xi\left(9\kappa^2 C^{\rm iso}_\ell + 3\kappa C^{\rm cor}_\ell\right)}. \tag{164}$$

Here $C^{\rm ad}_\ell$, $C^{\rm iso}_\ell$, and $C^{\rm cor}_\ell$ are the adiabatic, CDI, and correlated power spectra calculated for unity primordial spectra.

Note that this modulated curvaton model contains some simple special cases. For $\kappa = 0$, we have a purely adiabatic (i.e., scale-invariant) modulation. This is equivalent to a modulation of the scalar amplitude, $A_{\rm s}$. On the other hand, if we take the limit $\kappa \to \infty$, with fixed $\kappa^2\xi$ (i.e., with fixed isocurvature fraction $\beta_{\rm iso}$), we obtain a pure CDI modulation. For $\kappa = \xi = 0$ we have no modulation, i.e., we recover base ΛCDM. Therefore this model is particularly useful for examining a range of possible modulations within the context of a concrete framework.

In order to constrain this model, we use a formalism which was developed to determine the signatures of potential gradients in physical parameters in the CMB (Moss et al. 2011), and which is used to examine dipolar modulation and described in detail in Planck Collaboration XVI (2016). This approach is well-suited to testing the modulated curvaton model since it can accommodate scale-dependent modulations. Briefly, we write the temperature anisotropy covariance given a gradient ΔX_M in a parameter X as

$$C_{\ell m \ell' m'} = C_\ell \delta_{\ell\ell'}\delta_{mm'} + (-1)^m \frac{\delta C_{\ell\ell'}}{2} \left[(2\ell+1)(2\ell'+1)\right]^{1/2} \times \begin{pmatrix} \ell & \ell' & 1 \\ 0 & 0 & 0 \end{pmatrix} \sum_M \Delta X_M \begin{pmatrix} \ell & \ell' & 1 \\ -m & m' & M \end{pmatrix}, \tag{165}$$

where $\delta C_{\ell\ell'} \equiv {\rm d}C_\ell/{\rm d}X + {\rm d}C_{\ell'}/{\rm d}X$. Note that this covariance takes the form of Eqs. (157) and (158), with

$$C^1_{\ell;\ell'} = \frac{\delta C_{\ell\ell'}}{2} \left[(2\ell+1)(2\ell'+1)\right]^{1/2} \begin{pmatrix} \ell & \ell' & 1 \\ 0 & 0 & 0 \end{pmatrix}. \tag{166}$$

We then construct a maximum likelihood estimator for the gradient components. We use C^{-1} filtered data (Planck Collaboration XV 2016) and perform a mean-field subtraction, giving

$$\Delta\hat{X}_M = \frac{3}{f_{1M}} \sum_{\ell m \ell' m'} (-1)^m C^1_{\ell;\ell'} \begin{pmatrix} \ell & \ell' & 1 \\ -m & m' & M \end{pmatrix} \times \left(T_{\ell m} T^*_{\ell' m'} - \left\langle T_{\ell m} T^*_{\ell' m'} \right\rangle\right) \left[\sum_{\ell\ell'} \left(C^1_{\ell;\ell'}\right)^2 F_\ell F_{\ell'}\right]^{-1}. \quad (167)$$

Here f_{1M} is a normalization correction due to the applied mask, $M(\Omega)$, and is given by

$$f_{1M} \equiv \int \mathrm{d}\Omega\, Y^*_{1M}(\Omega) M(\Omega). \quad (168)$$

The $T_{\ell m}$ are the filtered data and $F_\ell \equiv \left\langle T_{\ell m} T^*_{\ell m} \right\rangle$. Note that the lack of aberration in the *Planck* Full Focal Plane simulations (Planck Collaboration XII 2016) is expected to have negligible effect on this analysis and on that of the quadrupolar modulation in the next subsection, since the CDI modulation is heavily suppressed for $\ell \gtrsim 500$, whereas the effect of aberration has a very different ℓ dependence and will bias the modulation signal for $\ell \lesssim 1000$ at an insignificant level.

In practice, exploring the parameter space of the model is sped up dramatically by binning the estimator defined in Eq. (167) into bins of width $\Delta\ell = 1$, which means that the estimators only need to be calculated once (Planck Collaboration XVI 2016). Finally, for the modulated curvaton model we identify

$$\frac{\mathrm{d}C_\ell}{\mathrm{d}X} = 2K_\ell C_\ell. \quad (169)$$

Note that for our constraints we fix the curvaton gradient to its maximum value, $\Delta\sigma_*/\sigma_* = 1$. Therefore, our constraints are conservative, since smaller $\Delta\sigma_*/\sigma_*$ would only reduce the modulation that this model could produce.

The temperature anisotropies measured by *Planck* constrain the modulated curvaton parameters κ and ξ via Eqs. (164) and (167). Figure 54 shows the constraints in this parameter space evaluating the estimator to $\ell_{\rm max} = 1000$. The maximum likelihood region corresponds to a band at $\kappa \gtrsim 3$. For parameters in this region, the model produces a large-scale asymmetry via a mainly-CDI modulation. However, the *amplitude* of this large-scale asymmetry is lower than the 6–7% actually observed (Planck Collaboration XVI 2016). The reason is that, had a CDI modulation produced all of the large-scale asymmetry, the consequent small-scale asymmetry (due to the shape of the scale-invariant CDI spectrum) would be larger than the *Planck* observations allow. The allowed CDI modulation is further reduced by the *Planck* 95% upper limit on an uncorrelated, scale-invariant ("axion"-type) isocurvature component, $\beta_{\rm iso} < 0.033$, from Sect. 11. Imposing this constraint reduces the available parameter space in the κ–ξ plane via Eq. (163), as illustrated in Fig. 54.

The best fit in Fig. 54 corresponds to $\Delta\chi^2 = -6.8$ relative to base ΛCDM, for two extra parameters. In order to assess how likely such an improvement would be in statistically isotropic skies, we note that the best-fit CDI modulation amplitude is very close to the mean amplitude expected due to cosmic variance, as calculated directly from Eq. (167). More precisely, since the amplitude is χ^2 distributed with three degrees of freedom, i.e., Maxwell-Boltzmann distributed, we conclude that about 44% of statistically isotropic skies will exhibit a measured

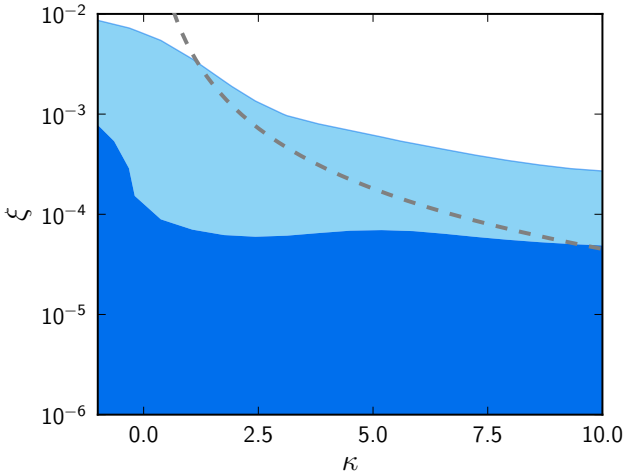

Fig. 54. 68% and 95% CL regions in the modulated isocurvature model parameter space using the *Planck* temperature data up to $\ell_{\rm max} = 1000$ (contours). The region above the dashed curve is ruled out by the *Planck* constraint on an uncorrelated, scale-invariant isocurvature component.

(via Eq. (167)) isocurvature modulation larger than that of the actual sky.

To summarize, the modulated curvaton model can only produce a small part of the observed large-scale asymmetry, and what it can produce is entirely consistent with cosmic variance in a statistically isotropic sky. Hence we must favour the base ΛCDM model over this model. Finally, note that further generalizing the model (e.g., to allow non-scale-invariant CDI spectra) may allow more large-scale asymmetry to be produced and hence result in an improved $\Delta\chi^2$, at the expense of more parameters. On the other hand, the neutrino isocurvature modes are not expected to fit the observed asymmetry well due to their approximate scale invariance (see Fig. 43).

12.4. Constraints on quadrupolar asymmetry generated during inflation

In this section we assume a quadrupolar directional dependence of the primordial scalar power spectrum about some axis $\pm\hat{\boldsymbol{d}}$ and having a scale-dependent amplitude $g(k)$. More specifically, we assume

$$\mathcal{P}_{\mathcal{R}}(\boldsymbol{k}) = \mathcal{P}^0_{\mathcal{R}}(k) \left\{1 + g(k) \left[\left(\hat{\boldsymbol{k}} \cdot \hat{\boldsymbol{d}}\right)^2 - \frac{1}{3}\right]\right\}, \quad (170)$$

which can be rewritten as

$$\mathcal{P}_{\mathcal{R}}(\boldsymbol{k}) = \mathcal{P}^0_{\mathcal{R}}(k) \left[1 + \sum_M g_{2M}(k)\, Y_{2M}(\hat{\boldsymbol{k}})\right], \quad (171)$$

where

$$g_{2M}(k) \equiv \frac{8\pi}{15} g(k)\, Y^*_{2M}(\hat{\boldsymbol{d}}), \quad (172)$$

with $g_{2M}(k)$ satisfying $g_{2,-M}(k) = (-1)^M g^*_{2M}(k)$. In this analysis, we will treat the modulation scale dependence as a power law, $g(k) = g_*(k/k_*)^q$, and consider five values of the spectral index, namely $q = -2$, -1, 0, 1, and 2. Importantly, for $q \neq 0$ our constraints on g_* will depend on the pivot scale, chosen as $k_* = 0.05\,\mathrm{Mpc}^{-1}$ as elsewhere in this paper. Models have been proposed predicting both positive and negative g_* (see, e.g. Tsujikawa 2014), so we keep the sign of g_* free.

Often in the literature the term $-g(k)/3$ is not included in the modulated power spectrum, Eq. (170). Our form sets the modulation monopole to zero, so that there is no correction to the isotropic power spectrum dependent on $g(k)$. We do this because for large $|q|$ the correction would require a joint analysis with the isotropic power spectrum likelihood. Inflationary models have been proposed which predict both forms. For example, the model in Ohashi et al. (2013) includes the modulation monopole, while the model in Libanov & Rubakov (2010) does not. For $q = 0$ our results apply to both forms due to the degeneracy of a scale-independent correction to $\mathcal{P}^0_{\mathcal{R}}(k)$ with the scalar amplitude, $A_{\rm s}$. However, for nonzero tilt a joint analysis would yield tighter constraints on g_* when the monopole correction is present, in which case our results will be conservative.

Given the anisotropic power spectrum of Eq. (171), the statistically anisotropic part of the CMB temperature fluctuations has the following expectation value (Ma et al. 2011):

$$C_{\ell,\ell';2,M} = i^{\ell-\ell'} D_{\ell\ell'} g_{2M}(k) \left[\frac{5(2\ell+1)(2\ell'+1)}{4\pi}\right]^{\frac{1}{2}} \times \begin{pmatrix} 2 & \ell & \ell' \\ 0 & 0 & 0 \end{pmatrix}, \quad (173)$$

where $D_{\ell\ell'} \equiv 4\pi \int \mathrm{d}\ln k\, \Delta^{\rm s}_{\ell,T}(k)\, \Delta^{\rm s}_{\ell',T}(k)\, \mathcal{P}^0_{\mathcal{R}}(k)(k/k_*)^q$ and $\Delta^{\rm s}_{\ell,T}(k)$ denotes the temperature radiation transfer function.

The analysis is carried out using the foreground-cleaned CMB temperature maps `Commander`, `NILC`, `SEVEM`, and `SMICA`, where we apply the extended common mask UT76. The implementation details of the optimal estimator can be found in Sect. 5.3 of Planck Collaboration XVI (2016). However, here we apply an inverse variance weighted filter that assumes a simple white noise component, but optimally accounts for the mask in the same manner as Planck Collaboration XVII (2014) and Sects. 6.3 and 6.6 of Planck Collaboration XVI (2016). We estimate g_{2M} from the data at multipoles $2 \le \ell \le 1200$. The range of multipoles is chosen such that the impact of foreground residuals on the conclusions is insignificant. Neglecting very small scales, however, sacrifices little constraining power because those scales are noise dominated. This conclusion was based on realistic simulations containing residual foregrounds. Moreover, we estimate the statistical uncertainty in g_{2M} with various $\ell_{\rm max}$ values using simulations.

Once we have obtained estimates for the five g_{2M} coefficients, we must determine values for the model parameters of interest, namely g_* and $\hat{\boldsymbol{d}}$. We assume the g_{2M} coefficients to be Gaussian distributed due to cosmic variance. We have explicitly checked this hypothesis with simulations. Hence the likelihood function is

$$\mathcal{L} \propto |G|^{-1/2} \times \exp\left[-\frac{1}{2}\left(\hat{g}_{2M} - g_{2M}(g_*, \hat{\boldsymbol{d}})\right)^{\mathsf{T}} G^{-1} \left(\hat{g}_{2M} - g_{2M}(g_*, \hat{\boldsymbol{d}})\right)\right], \quad (174)$$

where G is the g_{2M} covariance matrix, which is estimated using isotropic simulations. One approach to determining the model parameters would be to use this likelihood to calculate marginalized posterior distributions for g_*, from which mean values and errors could be determined. However, we find that g_* is so poorly constrained that the means and widths thus calculated strongly depend on the prior for g_*. Two sensible priors are uniform in g_* or proportional to g_*^2 [i.e., uniform in the Cartesian components of $(g_*, \hat{\boldsymbol{d}})$]. In addition, we find that the posterior means are much closer to zero then the widths, which is due to the approximate degeneracy between a modulation $(g_*, \hat{\boldsymbol{d}})$ and modulation $(-g_*, \hat{\boldsymbol{d}}')$, where $\hat{\boldsymbol{d}}'$ is orthogonal to $\hat{\boldsymbol{d}}$. In such a situation the degree of consistency between the measured value of g_* and the expectations of cosmic variance in statistically isotropic skies is unclear.

Instead we determine best-fit values for g_* and $\hat{\boldsymbol{d}}$ by maximizing the likelihood over the three parameters using a grid approach. To characterize how unexpected our best-fit values are in statistically isotropic skies, we repeat the procedure replacing our estimates for g_{2M} from the data with estimates from 1000 isotropic simulations. We finally calculate p-values, which give the fraction of simulations with a larger value of $|g_*|$ than the actual data. Note that from the Bayesian perspective the maximum-likelihood values amount to maximizing the posterior for g_* given a uniform prior on g_*, so that these values will change with a different prior. However, we have checked that the p-values depend only very weakly on the choice of prior.

Table 17 shows the g_* values obtained by minimizing χ^2 as well as the p-values for the data compared to statistically isotropic simulations. Note that the constraints on g_* are strongest for the most negative values of the exponent q. This is because for fixed g_* the largest asymmetry over the range of observable scales occurs for $q = -2$, at the largest scales, due to the location of the pivot scale, k_*. Our limits provide a stringent test of rotational symmetry during inflation. We find no sign of deviation from statistical isotropy.[25]

13. Combination with BICEP2/Keck Array-*Planck* cross-correlation

In this section we discuss the implications of the recent constraints on the primordial B-mode polarization from the cross-correlation of the BICEP2 and Keck Array data at 150 GHz with the *Planck* maps at higher frequencies to characterize and remove the contribution from polarized thermal dust emission from our Galaxy (BKP). On its own, the BKP likelihood leads to a 95% CL upper limit of $r < 0.12$, compatible with and independent of the constraints obtained using the 2015 *Planck* temperature and large angular scale polarization in Sect. 5. (Note, however, that the BKP likelihood uses the Hamimeche-Lewis approximation (Hamimeche & Lewis 2008), which requires the assumption of a fiducial model.) The BKP results are also compatible with the *Planck* 2013 Results (Planck Collaboration XVI 2014; Planck Collaboration XXII 2014). The posterior probability distribution for r obtained by BKP peaks away from zero at $r \approx 0.05$, but the region of large posterior probability includes $r = 0$.

Here we combine the baseline two-parameter BKP likelihood using the lowest five B-mode bandpowers with the *Planck* 2015 likelihoods. The two BKP nuisance parameters are the B-mode amplitude and frequency spectral index of the polarized thermal dust emission. The combined analysis yields the following constraint on the tensor-to-scalar ratio:

$$r_{0.002} < 0.08 \quad (95\%\ \mathrm{CL},\ \textit{Planck}\ \mathrm{TT{+}lowP{+}BKP}), \quad (175)$$

further improving on the upper limits obtained from the different data combinations presented in Sect. 5.

[25] The constraints from the *Planck* 2013 data by Kim & Komatsu (2013) should be multiplied by a factor of $\sqrt{2}$ in our normalization.

Table 17. Minimum-χ^2 g_* values for quadrupolar modulation, determined from the `Commander`, `NILC`, `SEVEM`, and `SMICA` foreground-cleaned maps.

	`Commander`		`NILC`		`SEVEM`		`SMICA`	
q	g_*	p-value [%]	g_*	p-value [%]	g_*	p-value [%]	g_*	p-value [%]
−2 ...	-7.39×10^{-5}	79.2	-7.66×10^{-5}	79.8	-7.43×10^{-5}	80.6	-7.52×10^{-5}	80.2
−1 ...	5.99×10^{-3}	97.3	6.65×10^{-3}	95.8	6.27×10^{-3}	97.2	6.22×10^{-3}	96.9
0 ...	-2.79×10^{-2}	12.5	-2.38×10^{-2}	26.9	-2.56×10^{-2}	20.7	-2.56×10^{-2}	20.0
1 ...	-2.15×10^{-2}	8.2	-1.79×10^{-2}	23.7	-1.93×10^{-2}	17.8	-1.93×10^{-2}	16.7
2 ...	-1.28×10^{-2}	9.7	-1.07×10^{-2}	23.7	-1.13×10^{-2}	20.4	-1.15×10^{-2}	18.1

Notes. Also given are p-values, defined as the fraction of simulations with larger $|g_*|$ than the data. These results demonstrate that the data are consistent with cosmic variance in statistically isotropic skies.

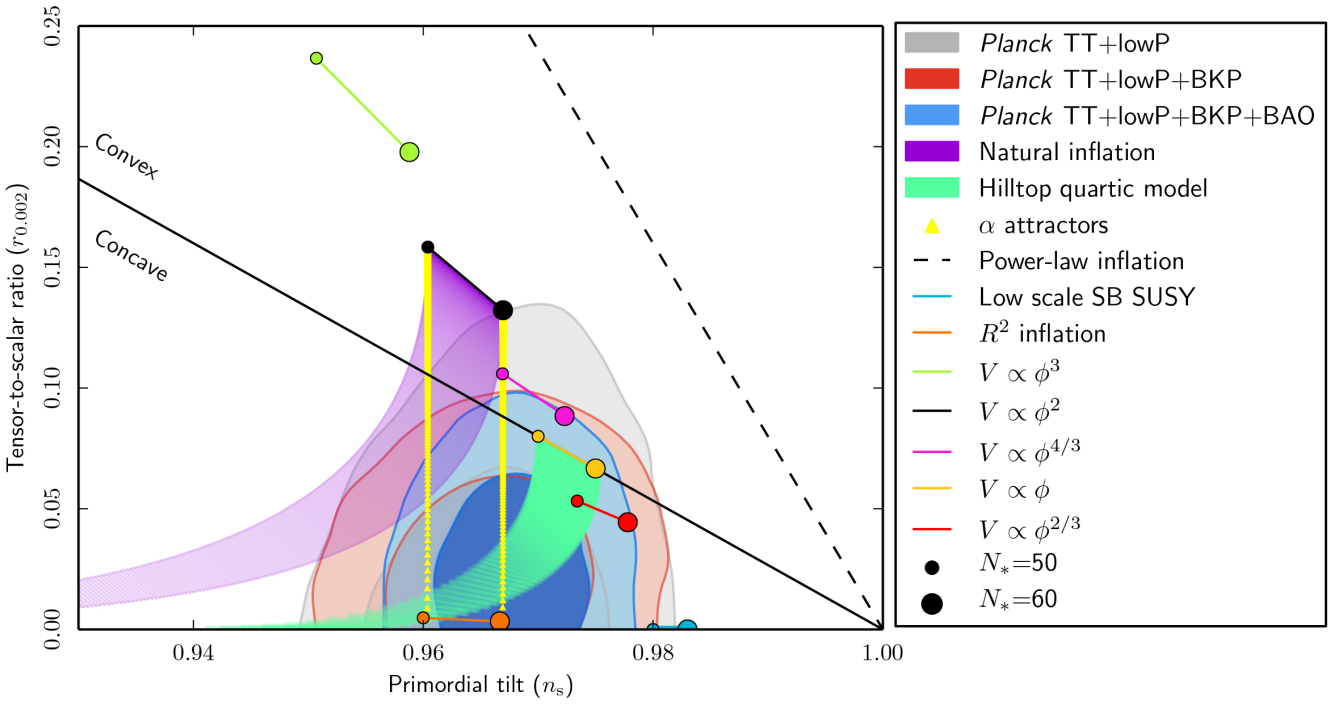

Fig. 55. Marginalized joint 68% and 95% CL regions for n_s and r at $k = 0.002\,\mathrm{Mpc}^{-1}$ from *Planck* alone and in combination with its cross-correlation with BICEP2/Keck Array and/or BAO data compared with the theoretical predictions of selected inflationary models. Note that the marginalized joint 68% and 95% CL regions have been obtained by assuming $\mathrm{d}n_s/\mathrm{d}\ln k = 0$.

By directly constraining the tensor mode, the BKP likelihood removes degeneracies between the tensor-to-scalar ratio and other parameters. Adding tensors and running, we obtain

$$r_{0.002} < 0.10 \quad (95\%\ \mathrm{CL},\ \textit{Planck}\ \mathrm{TT{+}lowP{+}BKP}), \qquad (176)$$

which constitutes almost a 50% improvement over the *Planck* TT+lowP constraint quoted in Eq. (27). These limits on tensor modes are more robust than the limits using the shape of the C_ℓ^{TT} spectrum alone because scalar perturbations cannot generate B modes irrespective of the shape of the scalar spectrum.

13.1. Implications of BKP on selected inflationary models

Using the BKP likelihood further strengthens the constraints on the inflationary parameters and models discussed in Sect. 6, as seen in Fig. 55. If we set $\epsilon_3 = 0$, the first slow-roll parameter is constrained to $\epsilon_1 < 0.0055$ at 95% CL by *Planck* TT+lowP+BKP. With the same data combination, concave potentials are preferred over convex potentials with $\ln B = 3.8$, which improves on the $\ln B = 2$ result obtained from the *Planck* data alone.

Combining with the BKP likelihood strengthens the constraints on the selected inflationary models studied in Sect. 6. Using the same methodology as in Sect. 6 and adding the BKP likelihood gives a Bayes factor preferring R^2 over chaotic inflation with monomial quadratic potential and natural inflation by odds of 403:1 and 270:1, respectively, under the assumption of a dust equation of state during the entropy generation stage. The combination with the BKP likelihood further penalizes the double-well model compared to R^2 inflation. However, adding BKP reduces the Bayes factor of the hilltop models compared to R^2, because these models can predict a value of the tensor-to-scalar ratio that better fits the statistically insignificant peak at $r \approx 0.05$. See Table 18 for the $\Delta\chi^2$ and the Bayes factors of inflationary models with the same two cases of post-inflationary

Table 18. Results of inflationary model comparison using the cross-correlation between BICEP2/Keck Array and *Planck*.

Inflationary model	$\Delta\chi^2$		$\ln B_{0X}$	
	$w_{\rm int}=0$	$w_{\rm int}\neq 0$	$w_{\rm int}=0$	$w_{\rm int}\neq 0$
$R+R^2/(6M^2)$	+2.1	+1.6	...	+0.3
$n=2/3$	+3.4	+3.0	−1.9	−1.2
$n=1$	+5.1	+5.1	−1.6	−1.8
$n=4/3$	+7.1	+6.6	−2.1	−2.5
$n=2$	+12.3	+11.8	−6.0	−5.6
$n=3$	+29.7	+29.6	−16.0	−15.6
$n=4$	+58.1	+58.0	−30.1	−29.9
Natural	+6.0	+5.2	−5.6	−5.0
Hilltop ($p=2$)	+1.6	+1.2	−0.7	−0.4
Hilltop ($p=4$)	+1.5	+1.0	−0.6	−0.9
Double well	+3.2	+3.1	−4.3	−4.2
Brane inflation ($p=2$)	+2.3	+2.2	+0.2	0.0
Brane inflation ($p=4$)	+2.2	+2.2	+0.1	−0.1
Exponential tails	+2.2	+1.4	−0.1	0.0
SB SUSY	+3.4	+1.6	−1.8	−1.5
Supersymmetric α-model	+1.6	+1.1	−1.1	+0.1
Superconformal ($m=1$)	+1.8	+1.3	−1.9	−1.4
Superconformal ($m\neq 1$)	+1.8	+0.9	−2.5	−2.2

Notes. This table is similar to Table 7, which did not use the BKP likelihood. Note, however, that the $\Delta\chi^2$ are computed with respect to the best fit of baseline + tensors, unlike in Table 7.

evolution studied in Sect. 6. Note, however, that the $\Delta\chi^2$ are computed with respect to the best fit of baseline + tensors, unlike in Table 7.

13.2. Implications of BKP on scalar power spectrum

The presence of tensors would, at least to some degree, require an enhanced suppression of the scalar power spectrum on large scales to account for the low-ℓ deficit in the $C_\ell^{\rm TT}$ spectrum. We therefore repeat the analysis of an exponential cutoff studied in Sect. 4.4 with tensor perturbations included and the standard tensor tilt (i.e., $n_{\rm t}=-r/8$). Allowing tensors does not significantly degrade the $\Delta\chi^2$ improvement found in Sect. 4.4 for *Planck* TT+lowP with a best fit at $r\approx 0$. When the BKP likelihood is combined, we obtain $\Delta\chi^2=-4$ with respect to the base ΛCDM model with a best fit at $r\approx 0.04$. However, since this model contains 3 additional parameters, it is not preferred over base ΛCDM.

In Fig. 56 we show how the scalar primordial power spectrum reconstruction discussed in Sect. 8.3 is modified when the BKP likelihood is also included. While the power spectrum reconstruction hardly varies given the uncertainties in the method, the trajectories of the slow-roll parameters are significantly closer to slow roll. When the 12-knot reconstruction is carried out, the upper bound on the tensor-to-scalar ratio is $r<0.11$ at 95% CL. The χ^2 per degree of freedom for the 5 low-k and 6 high-k knots are 1.14 and 0.22, respectively, corresponding to p-values of 0.33 and 0.97.

13.3. Relaxing the standard single-field consistency condition

We now relax the consistency condition (i.e., $n_{\rm t}=-r/8$) and allow the tensor tilt to be independent of the tensor-to-scalar ratio. This fully phenomenological analysis with the BKP likelihood

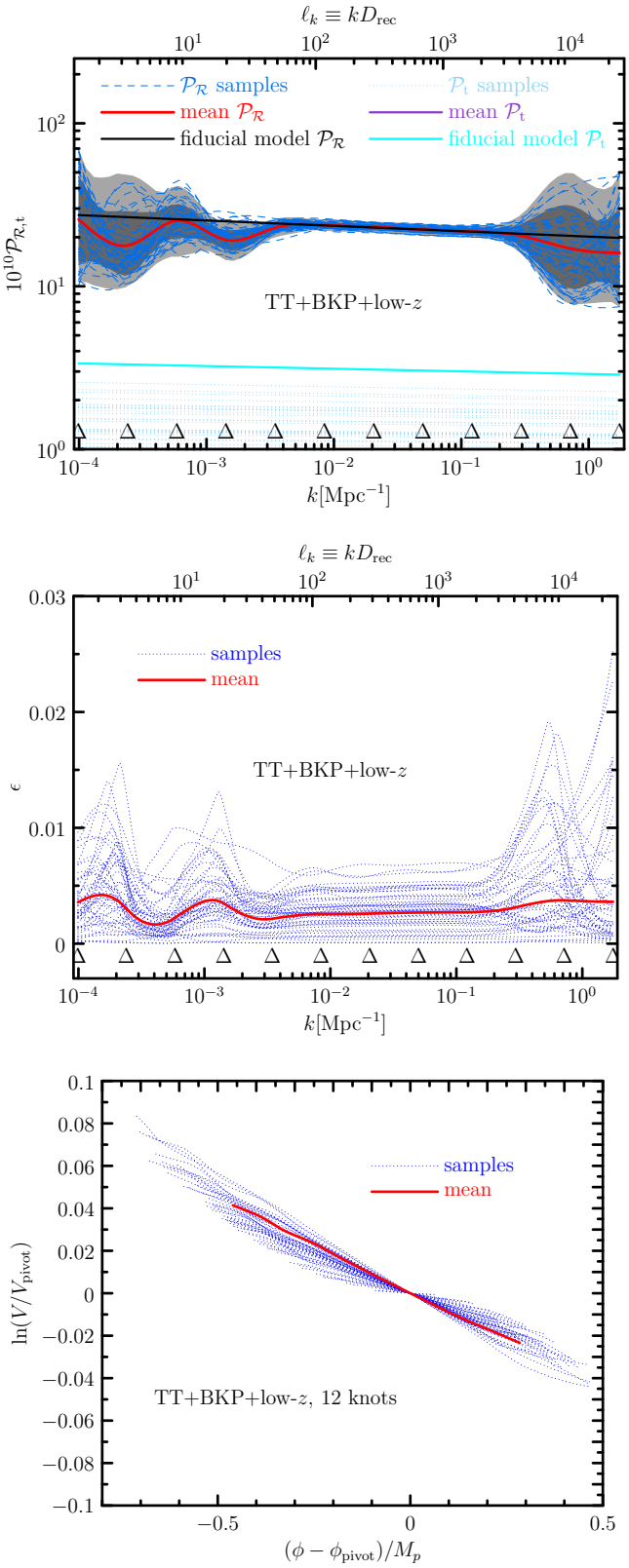

Fig. 56. Impact of BKP likelihood on scalar primordial power spectrum reconstruction. We show how including the BKP likelihood affects the reconstruction in Sect. 8.3. The *top panel* is to be compared with the reconstructions in Fig. 27, and we observe that including BKP has a minimal impact given the uncertainty in the reconstruction. The *middle panel* is to be compared with Fig. 31, and here we notice that including BKP excludes the trajectories with large values of ϵ. The *bottom panel* shows how the inflationary potential reconstructions are modified by BKP (to be compared with Fig. 32).

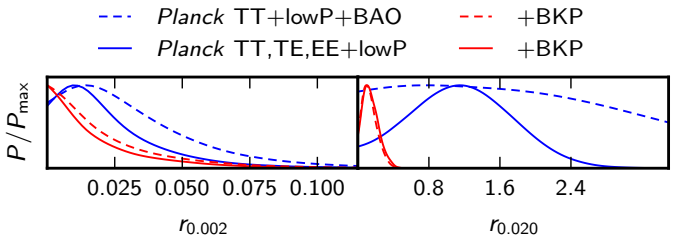

Fig. 57. Posterior probability density of the tensor-to-scalar ratio at two different scales. The inflationary consistency relation is relaxed and $r_{0.002}$ and $r_{0.020}$ are used as sampling parameters, assuming a power-law spectrum for primordial tensor perturbations. When the BKP likelihood is included in the analysis, the results with *Planck* TT+lowP+BAO and *Planck* TT, TE, EE+lowP coincide (dashed and solid red curves, respectively).

is complementary to the study of inflationary models with generalized Lagrangians in Sect. 10, which also predict modifications to the consistency condition $n_t = -r/8$ for a nearly scale-invariant spectrum of tensor modes. In this subsection we adopt a phenomenological approach, thereby including radical departures from $n_t \lesssim 0$, including values which are predicted in alternative models to inflation (Gasperini & Veneziano 1993; Boyle et al. 2004; Brandenberger et al. 2007). In Sect. 10 we folded in the *Planck* f_{NL} constraints (Planck Collaboration XVII 2016), whereas here we consider *Planck* and BKP likelihoods only. Complementary probes such as pulsar timing, direct detection of gravitational waves, and nucleosynthesis bounds could be used to constrain blue values for the tensor spectral index (Stewart & Brandenberger 2008), but here we are primarily interested in what CMB data can tell us.

We caution the reader that in the absence of a clear detection of a tensor component, joint constraints on r and n_t depend strongly on priors, or equivalently on the choice of parameterization. Nevertheless, the BKP likelihood has some constraining power over a range of scales more than a decade wide around $k \approx 0.01\,\mathrm{Mpc}^{-1}$, so the results are not entirely prior driven.

The commonly used (r, n_t) parameterization suffers from pathological behaviour around $r = 0$, which could be problematic for statistical sampling. We therefore use a parameterization specifying r at two different scales, (r_{k_1}, r_{k_2}) (analogous to the treatment of primordial isocurvature in Sect. 11) as well as the more familiar (r, n_t) parameterization. We present results based on $k_1 = 0.002\,\mathrm{Mpc}^{-1}$ and $k_2 = 0.02\,\mathrm{Mpc}^{-1}$, also quoting the amplitude at $k = 0.01\,\mathrm{Mpc}^{-1}$ for both parameterizations. This scale is close to the decorrelation scale for (r, n_t) for the *Planck*+BKP joint constraints. We obtain $r_{0.002} < 0.07$ (0.06) and $r_{0.02} < 0.29$ (0.31) at 95% CL from the two-scale parameterization with *Planck* TT+lowP+BAO+BKP (TT, TE, EE+lowP+BKP). Figure 57 illustrates the impact of the BKP likelihood on the one-dimensional posterior probabilities for these two parameters. The derived constraint at $k = 0.01\,\mathrm{Mpc}^{-1}$ is $r_{0.01} < 0.12$ (0.12) at 95% CL with *Planck* TT+lowP+BAO+BKP (TT, TE, EE+lowP+BKP). The upper panel of Fig. 58 shows the relevant 2D contours for the tensor-to-scalar ratios at the two scales and the improvement due to the combination with the BKP likelihood. The lower panel shows the 2D contours in $(r_{0.01}, n_t)$ obtained by sampling with the two-scale parameterization. Figure 59 shows the 2D contours in $(r_{0.01}, n_t)$ obtained by the $(r_{0.002}, n_t)$ parameterization.

We conclude that positive values of the tensor tilt, n_t, are not statistically significantly preferred by the BKP joint measurement of B-mode polarization in combination with

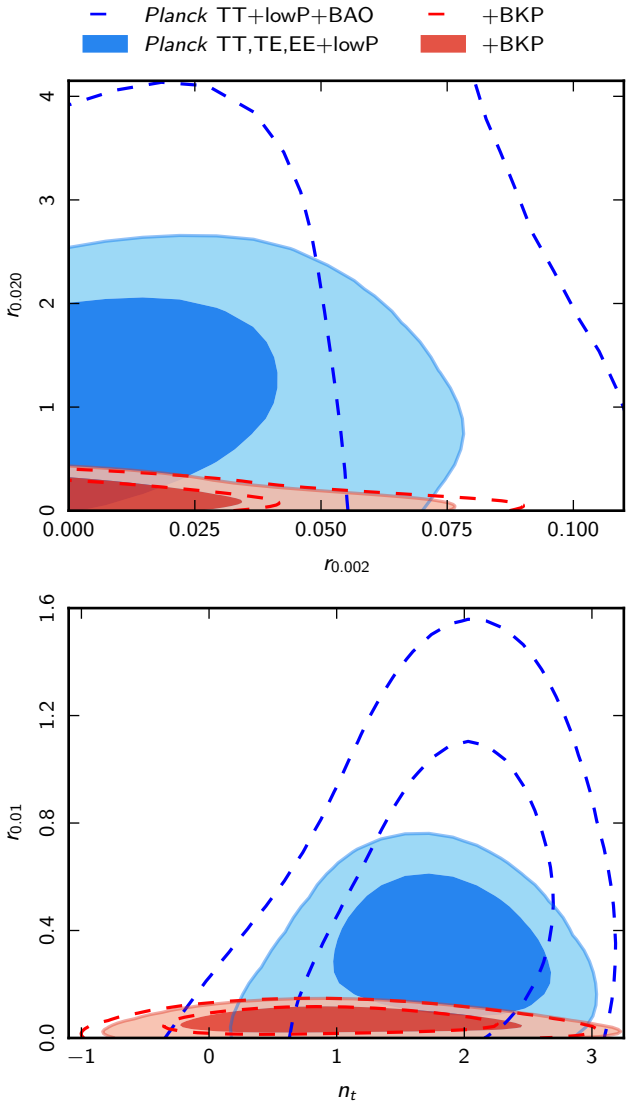

Fig. 58. 68% and 95% CL constraints on tensors when the inflationary consistency relation is relaxed, with *Planck* TT+lowP+BAO (blue dashed contours) and TT, TE, EE+lowP (blue shaded regions). The red colours are for the same data plus the BKP joint likelihood. The *upper panel* shows our independent primary parameters $r_{0.002}$ and $r_{0.020}$. The lower panel shows the derived parameters n_t and $r_{0.01}$. The scale $k = 0.01\,\mathrm{Mpc}^{-1}$ is near the decorrelation scale of (n_t, r) for the *Planck*+BKP data.

Planck data, a conclusion at variance with results reported using the BICEP2 data (Gerbino et al. 2014). However, the now firmly established contamination by polarized dust emission easily explains the discrepancy. Values of tensor tilt consistent with the standard single-field inflationary consistency relation are compatible with the *Planck*+BKP constraints.

14. Conclusions

The *Planck* full mission temperature and polarization data are consistent with the spatially flat base ΛCDM model whose perturbations are Gaussian and adiabatic with a spectrum described by a simple power law, as predicted by the simplest inflationary models. For this release, the basic *Planck* results do not rely on external data. The first *Planck* polarization release at large

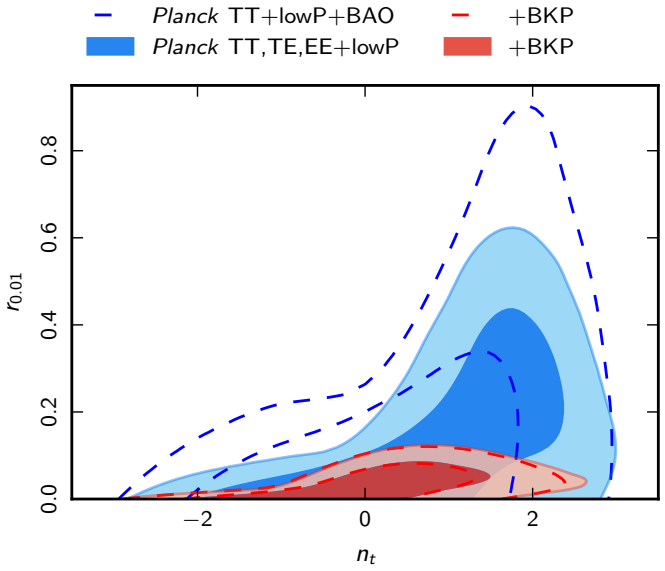

Fig. 59. The same as Fig. 58 lower panel, but using n_t and $r_{0.002}$ as primary parameters.

angular scales from the LFI 70 GHz channel determines an optical depth of $\tau = 0.067 \pm 0.022$ (68% CL, *Planck* low multipole likelihood), a value smaller than the previous *Planck* 2013 result based on the WMAP9 polarization likelihood as delivered by the WMAP team. This *Planck* value of τ is consistent with an analysis of WMAP9 polarization data cleaned for polarized dust emission using the *Planck* 353 GHz data (Planck Collaboration XV 2014; Planck Collaboration XI 2016). The estimates of cosmological parameters from the full mission temperature data and polarization on large angular scales are consistent with those of the *Planck* 2013 release. The TE and EE spectra at $\ell \geq 30$ together with the lensing power spectrum lead to cosmological constraints in agreement with those obtained from temperature.

The *Planck* full mission temperature and large-angular-scale polarization data rule out an exactly scale-invariant spectrum of curvature perturbations at $5.6\,\sigma$. For the base ΛCDM model, the spectral index is measured to be $n_s = 0.965 \pm 0.006$ (68% CL, *Planck* TT+lowP). No evidence for a running of the spectral index is found, with $\mathrm{d}n_s/\mathrm{d}\ln k = -0.008 \pm 0.008$ (68% CL, *Planck* TT+lowP). By considering *Planck* TT+lowP+lensing we obtain $n_s = 0.968 \pm 0.006$ and $\mathrm{d}n_s/\mathrm{d}\ln k = -0.003 \pm 0.007$, both at 68% CL.

The *Planck* full mission data improve the upper bound on the tensor-to-scalar ratio to $r_{0.002} < 0.10$ (95% CL, *Planck* TT+lowP), a bound that changes only slightly when including the *Planck* lensing likelihood, the high-ℓ polarization likelihood, or the likelihood from the WMAP large-angular-scale polarization map (dust-cleaned with the *Planck* 353 GHz map). We showed how the low-ℓ deficit in temperature contributes to the *Planck* upper bound on $r_{0.002}$, but this deficit is not a statistically significant anomaly within the base ΛCDM cosmology. Using the full mission *Planck* data, we find the upper bound on $r_{0.002}$ stable, even when extended cosmological models or models with CDM isocurvature are considered. The *Planck* bound on $r_{0.002}$ is consistent with the recent result $r_{0.002} < 0.12$ at 95% CL obtained by the BICEP2/Keck Array-*Planck* cross-correlation analysis (BKP) which provides an estimate for the contamination from polarized dust emission (Planck Collaboration XXX 2014). By combining *Planck* TT+lowP with the BKP cross-correlation likelihood, we obtain $r_{0.002} < 0.08$ at 95% CL.

The increased precision of the *Planck* full mission data reduces the area enclosed by the 95% confidence contour in the (n_s, r) plane by 29%. We performed a Bayesian model comparison with the same methodology as in PCI13, taking into account reheating uncertainties by marginalizing over two extra parameters: the energy scale at thermalization, $\rho_{\rm th}$, and the parameter $w_{\rm int}$ characterizing the average equation of state between the end of inflation and thermalization. Among the models considered using this approach, the R^2 inflationary model proposed by Starobinsky (1980) is the most favoured. Due to its high tensor-to-scalar ratio, the quadratic model is now strongly disfavoured with respect to R^2 inflation for *Planck* TT+lowP in combination with BAO data. By further including the BKP likelihood, this conclusion is confirmed, and natural inflation is also disfavoured.

We reconstructed the inflaton potential and the Hubble parameter evolution during the observable part of inflation using a Taylor expansion of the inflaton potential or $H(\phi)$. This analysis did not rely on the slow-roll approximation, nor on any assumption about the end of inflation. When higher-order terms were allowed, both reconstructions led to a change in the slope of the potential at the beginning of the observable range, thus better fitting the low-ℓ temperature deficit by turning on a non-zero running of running and accommodating $r_{0.002} \approx 0.2$. These models, however, are not significantly favoured compared to lower-order parameterizations that lead to slow-roll evolution at all times.

Three distinct methods were used to reconstruct the primordial power spectrum. All three methods strongly constrain deviations from a featureless power spectrum over the range of scales $0.008\,\mathrm{Mpc}^{-1} \lesssim k \lesssim 0.1\,\mathrm{Mpc}^{-1}$. More interestingly, they also independently find common patterns in the primordial power spectrum of curvature perturbations $\mathcal{P}_{\mathcal{R}}(k)$ at $k \lesssim 0.008\,\mathrm{Mpc}^{-1}$. These patterns are related to the dip at $\ell \approx 20$–40 in the temperature power spectrum. This deviation from a simple power-law spectrum has weak statistical significance due to the large cosmic variance at low ℓ.

This direct reconstruction of the power spectrum is complemented by a search for parameterized features in physically motivated models. The models considered range from the minimal case of a kinetic-energy-dominated phase preceding a short inflationary stage (with just one extra parameter), to a model with a step-like feature in the potential and in the sound speed (with five extra parameters). As with the *Planck* 2013 nominal mission data, these templates lead to an improved fit, up to $\Delta\chi^2 \approx 12$. However, neither Bayesian model comparison nor a frequentist-simulation-based analysis shows any statistically significant preference over a simple power law.

We have updated the analysis that combines power spectrum constraints with those derived from the $f_{\rm NL}$ parameters (Planck Collaboration XVII 2016). New limits on the sound speed inferred from the full mission temperature and polarization data further constrain the slow-roll parameters for generalized models, including DBI inflation. For the first time, we derived combined constraints on Galileon inflation, including the region of parameter space in which the predicted spectrum of gravitational waves has a blue spectral index.

Several models motivated by the axion monodromy mechanism in string theory predict oscillatory modulations and corresponding non-Gaussianities, potentially detectable by *Planck*. A TT-only analysis picks up four possible modulation frequencies, which remain present when the high-ℓ polarization likelihood is included. An inspection of frequency residuals in the high-ℓ *TT* likelihood does not reveal evidence of foreground-related systematics at similar frequencies. However, a Bayesian model comparison analysis prefers the smooth base ΛCDM model over

modulated models, suggesting that the latter could simply be fitting the noise in the data. The monodromy model predicts resonant non-Gaussian features correlated to power spectrum features. A partial analysis beyond the power spectrum was presented. We also constrained a possible pseudo-coupling of the axion to gauge fields by requiring that non-Gaussianities induced by inverse decay satisfy the *Planck* bounds on $f_{\rm NL}$.

Section 11 reports on a search for possible deviations from purely adiabatic initial conditions by studying a range of models including isocurvature modes as well as possible correlations with the adiabatic mode. The *Planck* full mission temperature data are consistent with adiabaticity. The *Planck TT* data place tight constraints on three-parameter extensions to the flat adiabatic base ΛCDM model, allowing arbitrarily-correlated mixtures of the adiabatic mode with one isocurvature mode (of either the CDM, baryon, neutrino density, or neutrino velocity type). Adding the high-ℓ *TE* and *EE* polarization data further squeezes the constraints, since polarization spectra contain additional shape and phase information on acoustic oscillations. The likelihood with polarization included is in agreement with adiabatic initial conditions. However, the tightening of the constraints after including polarization must be interpreted with caution because of possible systematic effects. For this reason we emphasize the more conservative *Planck* TT+lowP bounds in Table 16. The constraints on the six base-ΛCDM cosmological model parameters remain stable when correlated isocurvature modes are allowed. The largest shifts occur for the neutrino density mode, but these shifts are not significant (i.e., are below 1σ). The constraints on the tensor-to-scalar ratio also remain stable when isocurvature modes are allowed.

Finally we examined the connection between inflation and statistical isotropy, a key prediction of the simplest inflationary models. We tested separately the two lowest moments of an anisotropic modulation of the primordial curvature power spectrum. We found that a modulated curvaton model proposed to explain the observed large-scale dipolar power asymmetry cannot account for all of the asymmetry, and hence is not preferred over statistically isotropic base ΛCDM. The full mission temperature data place the tightest constraints to date on a quadrupolar modulation of curvature perturbations.

Acknowledgements. The Planck Collaboration acknowledges the support of: ESA; CNES and CNRS/INSU-IN2P3-INP (France); ASI, CNR, and INAF (Italy); NASA and DoE (USA); STFC and UKSA (UK); CSIC, MINECO, JA, and RES (Spain); Tekes, AoF, and CSC (Finland); DLR and MPG (Germany); CSA (Canada); DTU Space (Denmark); SER/SSO (Switzerland); RCN (Norway); SFI (Ireland); FCT/MCTES (Portugal); ERC and PRACE (EU). A description of the Planck Collaboration and a list of its members, indicating which technical or scientific activities they have been involved in, can be found at http://www.cosmos.esa.int/web/planck/planck-collaboration. This research used resources of the National Energy Research Scientific Computing Center, a DOE Office of Science User Facility supported by the Office of Science of the US Department of Energy under Contract No. DE-AC02-05CH11231. Part of this work was undertaken at the STFC DiRAC HPC Facilities at the University of Cambridge, funded by UK BIS National E-infrastructure capital grants. We gratefully acknowledge the IN2P3 Computer Center (http://cc.in2p3.fr) for providing a significant amount of the computing resources and services needed for this work.

References

Achúcarro, A., Gong, J.-O., Hardeman, S., Palma, G. A., & Patil, S. P. 2011, JCAP, 1101, 030
Ackerman, L., Carroll, S. M., & Wise, M. B. 2007, Phys. Rev. D, 75, 083502
Adams, F. C., Bond, J. R., Freese, K., Frieman, J. A., & Olinto, A. V. 1993, Phys. Rev. D, 47, 426
Adams, J. A., Cresswell, B., & Easther, R. 2001, Phys. Rev. D, 64, 123514
Agarwal, N., & Bean, R. 2009, Phys. Rev. D, 79, 023503
Alishahiha, M., Silverstein, E., & Tong, D. 2004, Phys. Rev. D, 70, 123505
Amendola, L., Gordon, C., Wands, D., & Sasaki, M. 2002, Phys. Rev. Lett., 88, 211302
Anber, M. M., & Sorbo, L. 2010, Phys. Rev. D, 81, 043534
Anderson, L., Aubourg, E, Bailey, S., et al. 2014, MNRAS, 441, 24
Armendáriz-Picón, C., Damour, T., & Mukhanov, V. 1999, Phys. Lett. B, 458, 209
Aslanyan, G., Price, L. C., Abazajian, K. N., & Easther, R. 2014, JCAP, 08, 052
Audren, B., Lesgourgues, J., Benabed, K., & Prunet, S. 2013, JCAP, 1302, 001
Barnaby, N., & Peloso, M. 2011, Phys. Rev. Lett., 106, 181301
Barnaby, N., Pajer, E., & Peloso, M. 2012, Phys. Rev. D, 85, 023525
Bartolo, N., Matarrese, S., Peloso, M., & Ricciardone, A. 2013, JCAP, 1308, 022
Bartolo, N., Matarrese, S., & Riotto, A. 2001, Phys. Rev. D, 64, 123504
Bartolo, N., Matarrese, S., & Riotto, A. 2004a, Phys. Rev. Lett., 93, 231301
Babich, D., Creminelli, P., & Zaldarriaga, M. 2004, JCAP, 8, 9
Barnaby, N., Namba, R., & Peloso, M. 2011, JCAP, 4, 9
Bartolo, N., & Liddle, A. R. 2002, Phys. Rev. D, 65, 121301
Bartolo, N., Matarrese, S., & Riotto, A. 2004b, Phys. Rev. D, 69, 043503
Barvinsky, A. O., Kamenshchik, A. Y., & Starobinsky, A. A. 2008, JCAP, 0811, 021
Baumann, D., Green, D., & Porto, R. A. 2015, JCAP, 1, 16
Bean, R., Chen, X., Peiris, H., & Xu, J. 2008, Phys. Rev. D, 77, 023527
Becker, R. H., Fan, X., White, R. L., et al. 2001, AJ, 122, 2850
Beltrán, M., García-Bellido, J., Lesgourgues, J., & Viel, M. 2005, Phys. Rev. D, 72, 103515
Bennett, C. L., Hill, R. S., Hinshaw, G., et al. 2011, ApJS, 192, 17
Berera, A. 1995, Phys. Rev. Lett., 75, 3218
Beutler, F., Blake, C., Colless, M., et al. 2011, MNRAS, 416, 3017
Bezrukov, F., & Shaposhnikov, M. 2008, Phys. Lett. B, 659, 703
Bezrukov, F., & Shaposhnikov, M. 2009, JHEP, 07, 089
BICEP2 Collaboration. 2014a, ApJ, 792, 62
BICEP2 Collaboration. 2014b, Phys. Rev. Lett., 112, 241101
BICEP2/Keck Array and Planck Collaborations. 2015, Phys. Rev. Lett., 114, 101301
Binétruy, P., Kiritsis, E., Mabillard, J., Pieroni, M., & Rosset, C. 2015, J. Cosmol. Astropart. Phys., 2015, 33
Blas, D., Lesgourgues, J., & Tram, T. 2011, JCAP, 1107, 034
Boubekeur, L., & Lyth, D. 2005, JCAP, 0507, 010
Boyle, L. A., Steinhardt, P. J., & Turok, N. 2004, Phys. Rev. D, 69, 127302
Bozza, V., Giovannini, M., & Veneziano, G. 2003, JCAP, 0305, 001
Brandenberger, R. H., Nayeri, A., Patil, S. P., & Vafa, C. 2007, Phys. Rev. Lett., 98, 231302
Bucher, M. 2015, Int. J. Mod. Phys. D, 24, 1530004
Bucher, M., Moodley, K., & Turok, N. 2000, Phys. Rev. D, 62, 083508
Bucher, M., Moodley, K., & Turok, N. 2001, Phys. Rev. Lett., 87, 191301
Buchmüller, W., Domcke, V., & Kamada, K. 2013, Phys. Lett., B726, 467
Burgess, C., Martineau, P., Quevedo, F., Rajesh, G., & Zhang, R. 2002, JHEP, 0203, 052
Burrage, C., de Rham, C., Seery, D., & Tolley, A. J. 2011, JCAP, 1, 14
Byrnes, C. T., & Wands, D. 2006, Phys. Rev. D, 74, 043529
Casadio, R., Finelli, F., Kamenshchik, A., Luzzi, M., & Venturi, G. 2006, JCAP, 0604, 011
Chen, X. 2005a, JHEP, 8, 45
Chen, X. 2005b, Phys. Rev. D, 71, 063506
Chen, X. 2005c, Phys. Rev. D, 72, 123518
Chen, X., Huang, M.-X., Kachru, S., & Shiu, G. 2007, JCAP, 1, 2
Chen, X., Easther, R., & Lim, E. A. 2008, JCAP, 0804, 010
Chluba, J., Hamann, J., & Patil, S. P. 2015, Int. J. Mod. Phys. D, 24, 1530023
Choe, J., Gong, J.-O., & Stewart, E. D. 2004, JCAP, 0407, 012
Cicoli, M., Burgess, C., & Quevedo, F. 2009, JCAP, 0903, 013
Contaldi, C. R., Peloso, M., Kofman, L., & Linde, A. D. 2003, JCAP, 0307, 002
Copeland, E. J., Liddle, A. R., Lyth, D. H., Stewart, E. D., & Wands, D. 1994, Phys. Rev. D, 49, 6410
Creminelli, P., D'Amico, G., Musso, M., Noreña, J., & Trincherini, E. 2011, JCAP, 2, 6
Danielsson, U. H. 2002, Phys. Rev. D, 66, 023511
De Felice, A., & Tsujikawa, S. 2013, JCAP, 3, 30
de Rham, C., & Gabadadze, G. 2010a, Phys. Rev. D, 82, 044020
de Rham, C., & Gabadadze, G. 2010b, Phys. Lett. B, 693, 334
Deffayet, C., Deser, S., & Esposito-Farèse, G. 2009a, Phys. Rev. D, 80, 064015
Deffayet, C., Esposito-Farèse, G., & Vikman, A. 2009b, Phys. Rev. D, 79, 084003
Dimastrogiovanni, E., Bartolo, N., Matarrese, S., & Riotto, A. 2010, Adv.

Astron., 752670
Dvali, G., & Tye, S. H. 1999, Phys. Lett. B, 450, 72
Dvali, G. R., Shafi, Q., & Schaefer, R. K. 1994, Phys. Rev. Lett., 73, 1886
Dvali, G., Shafi, Q., & Solganik, S. 2001, ArXiv e-prints [arXiv:hep-th/0105203]
Easther, R., & Flauger, R. 2014, JCAP, 1402, 037
Easther, R., & Peiris, H. 2006, JCAP, 0609, 010
Easther, R., & Peiris, H. V. 2012, Phys. Rev. D, 85, 103533
Easther, R., Kinney, W. H., & Peiris, H. 2005, JCAP, 0505, 009
Eisenstein, D. J., Zehavi, I., Hogg, D. W., et al. 2005, ApJ, 633, 560
Ellis, J., Nanopoulos, D. V., & Olive, K. A. 2013a, Phys. Rev. Lett., 111, 111301
Ellis, J., Nanopoulos, D. V., & Olive, K. A. 2013b, JCAP, 1310, 009
Enqvist, K., & Sloth, M. S. 2002, Nucl. Phys. B, 626, 395
Enqvist, K., Kurki-Suonio, H., & Valiviita, J. 2002, Phys. Rev. D, 65, 043002
Erickcek, A. L., Hirata, C. M., & Kamionkowski, M. 2009, Phys. Rev. D, 80, 083507
Farakos, F., Kehagias, A., & Riotto, A. 2013, Nucl. Phys. B, 876, 187
Feroz, F., & Hobson, M. 2008, MNRAS, 384, 449
Feroz, F., Hobson, M., & Bridges, M. 2009, MNRAS, 398, 1601
Feroz, F., Hobson, M., Cameron, E., & Pettitt, A. 2013, ArXiv e-prints [arXiv:1306.2144]
Ferrara, S., Kallosh, R., Linde, A., & Porrati, M. 2013a, Phys. Rev. D, 88, 085038
Ferrara, S., Kallosh, R., & Van Proeyen, A. 2013b, JHEP, 1311, 134
Ferreira, R. Z., & Sloth, M. S. 2014, JHEP, 12, 139
Finelli, F., Hamann, J., Leach, S. M., & Lesgourgues, J. 2010, JCAP, 1004, 011
Flauger, R., Hill, J. C., & Spergel, D. N. 2014a, JCAP, 1408, 039
Flauger, R., & Pajer, E. 2011, JCAP, 1101, 017
Flauger, R., McAllister, L., Silverstein, E., & Westphal, A. 2014b, ArXiv e-prints [arXiv:1412.1814]
Freese, K., Frieman, J. A., & Olinto, A. V. 1990, Phys. Rev. Lett., 65, 3233
Gao, X., & Steer, D. A. 2011, JCAP, 12, 19
Garcia-Bellido, J., & Roest, D. 2014, Phys. Rev. D, 89, 103527
García-Bellido, J., & Wands, D. 1996, Phys. Rev. D, 53, 5437
Garcia-Bellido, J., Rabadan, R., & Zamora, F. 2002, JHEP, 0201, 036
Garriga, J., & Mukhanov, V. F. 1999, Phys. Lett. B, 458, 219
Gasperini, M., & Veneziano, G. 1993, Astropart. Phys., 1, 317
Gauthier, C., & Bucher, M. 2012, JCAP, 1210, 050
Gerbino, M., Marchini, A., Pagano, L., et al. 2014, Phys. Rev. D, 90, 047301
Goncharov, A., & Linde, A. D. 1984, Sov. Phys. JETP, 59, 930
Gong, J.-O., & Stewart, E. D. 2001, Phys. Lett. B, 510, 1
Gorbunov, D., & Panin, A. 2011, Phys. Lett. B, 700, 157
Gordon, C., & Lewis, A. 2003, Phys. Rev. D, 67, 123513
Gordon, C., Wands, D., Bassett, B. A., & Maartens, R. 2001, Phys. Rev. D, 63, 023506
Górski, K. M., Hivon, E., Banday, A. J., et al. 2005, ApJ, 622, 759
Grin, D., Hanson, D., Holder, G. P., Doré, O., & Kamionkowski, M. 2014, Phys. Rev. D, 89, 023006
Guth, A. H., Kaiser, D. I., & Nomura, Y. 2014, Phys. Lett. B, 733, 112
Habib, S., Heitmann, K., Jungman, G., & Molina-Paris, C. 2002, Phys. Rev. Lett., 89, 281301
Hamann, J., Lesgourgues, J., & Valkenburg, W. 2008, JCAP, 0804, 016
Hamimeche, S., & Lewis, A. 2008, Phys. Rev. D, 77, 103013
Handley, W. J., Hobson, M. P., & Lasenby, A. N. 2015, MNRAS, 450, L61
Harrison, E. R. 1970, Phys. Rev. D, 1, 2726
Hu, W., Seljak, U., White, M. J., & Zaldarriaga, M. 1998, Phys. Rev. D, 57, 3290
Hu, W., & White, M. J. 1997, Phys. Rev. D, 56, 596
Ijjas, A., Steinhardt, P. J., & Loeb, A. 2013, Phys. Lett. B, 723, 261
Ijjas, A., Steinhardt, P. J., & Loeb, A. 2014, Phys. Lett. B, 736, 142
Jackson, M. G., & Shiu, G. 2013, Phys. Rev. D, 88, 123511
Jackson, M. G., Wandelt, B., & Bouchet, F. 2014, Phys. Rev. D, 89, 023510
Kachru, S., Kallosh, R., Linde, A. D., et al. 2003, JCAP, 0310, 013
Kaiser, D. I., & Sfakianakis, E. I. 2014, Phys. Rev. Lett., 112, 011302
Kallosh, R., & Linde, A. 2013a, JCAP, 1310, 033
Kallosh, R., & Linde, A. 2013b, JCAP, 1306, 028
Kallosh, R., Linde, A., & Roest, D. 2013, JHEP, 1311, 198
Kaloper, N., Lawrence, A., & Sorbo, L. 2011, JCAP, 1103, 023
Kamionkowski, M., Kosowsky, A., & Stebbins, A. 1997, Phys. Rev. D, 55, 7368
Kanno, S., Sasaki, M., & Tanaka, T. 2013, Progr. Theor. Exp. Phys., 2013, 111E01
Kawasaki, M., & Sekiguchi, T. 2008, Prog. Theor. Phys., 120, 995
Ketov, S. V., & Starobinsky, A. A. 2011, Phys. Rev. D, 83, 063512
Kim, J., & Komatsu, E. 2013, Phys. Rev. D, 88, 101301
Kim, J. E., Nilles, H. P., & Peloso, M. 2005, JCAP, 0501, 005
Kinney, W. H. 2002, Phys. Rev. D, 66, 083508
Kinney, W. H., Kolb, E. W., Melchiorri, A., & Riotto, A. 2006, Phys. Rev. D, 74, 023502
Kobayashi, T., & Takahashi, F. 2011, JCAP, 1101, 026
Kobayashi, T., Yamaguchi, M., & Yokoyama, J. 2010, Phys. Rev. Lett., 105, 231302
Kobayashi, T., Yamaguchi, M., & Yokoyama, J. 2011a, Progr. Theor. Phys., 126, 511
Kobayashi, T., Yamaguchi, M., & Yokoyama, J. 2011b, Phys. Rev. D, 83, 103524
Kosowsky, A., & Turner, M. S. 1995, Phys. Rev. D, 52, 1739
Langlois, D. 1999, Phys. Rev. D, 59, 123512
Langlois, D., & Riazuelo, A. 2000, Phys. Rev. D, 62, 043504
Leach, S. M., Liddle, A. R., Martin, J., & Schwarz, D. J. 2002, Phys. Rev. D, 66, 023515
Lesgourgues, J. 2011, ArXiv e-prints [arXiv:1104.2932]
Lesgourgues, J., & Valkenburg, W. 2007, Phys. Rev. D, 75, 123519
Lesgourgues, J., Polarski, D., Prunet, S., & Starobinsky, A. A. 2000, Astron. Astrophys., 359, 414
Lesgourgues, J., Starobinsky, A. A., & Valkenburg, W. 2008, JCAP, 0801, 010
Lewis, A., & Bridle, S. 2002, Phys. Rev. D, 66, 103511
Libanov, M., & Rubakov, V. 2010, JCAP, 1011, 045
Liddle, A. R., & Cortês, M. 2013, Phys. Rev. Lett., 111, 111302
Linde, A. 2014, ArXiv e-prints [arXiv:1402.0526]
Linde, A. D. 1983, Phys. Lett. B, 129, 177
Linde, A. D. 1994, Phys. Rev. D, 49, 748
Linde, A. D., & Mukhanov, V. 2006, JCAP, 0604, 009
Linde, A. D., & Mukhanov, V. F. 1997, Phys. Rev. D, 56, 535
Liddle, A. R., & Leach, S. M. 2003, Phys. Rev. D, 68, 103503
Linde, A., Mooij, S., & Pajer, E. 2013, Phys. Rev. D, 87, 103506
Lorenz, L., Martin, J., & Ringeval, C. 2008, Phys. Rev. D, 78, 083513
Lyth, D. H. 2013, JCAP, 1308, 007
Lyth, D. H., & Wands, D. 2002, Phys. Lett. B, 524, 5
Lyth, D. H., Ungarelli, C., & Wands, D. 2003, Phys. Rev. D, 67, 023503
Ma, C.-P., & Bertschinger, E. 1995, ApJ, 455, 7
Ma, Y.-Z., Efstathiou, G., & Challinor, A. 2011, Phys. Rev. D, 83, 083005
Ma, Y.-Z., Huang, Q.-G., & Zhang, X. 2013, Phys. Rev. D, 87, 103516
Maleknejad, A., Sheikh-Jabbari, M., & Soda, J. 2013, Phys. Rept., 528, 161
Martin, J., & Brandenberger, R. H. 2001, Phys. Rev. D, 63, 123501
Martin, J., & Ringeval, C. 2010, Phys. Rev. D, 82, 023511
Martin, J., & Schwarz, D. J. 2003, Phys. Rev. D, 67, 083512
Martin, J., Ringeval, C., & Vennin, V. 2014, Phys. Dark Univ., 5-6, 75
McAllister, L., Silverstein, E., & Westphal, A. 2010, Phys. Rev. D, 82, 046003
McAllister, L., Silverstein, E., Westphal, A., & Wrase, T. 2014, JHEP, 1409, 123
Meerburg, P. D. 2014, Phys. Rev. D, 90, 063529
Meerburg, P. D., & Pajer, E. 2013, JCAP, 2, 17
Meerburg, P. D., & Spergel, D. N. 2014, Phys. Rev. D, 89, 063537
Meerburg, P. D., Spergel, D. N., & Wandelt, B. D. 2014a, ArXiv e-prints [arXiv:1406.0548]
Meerburg, P. D., Spergel, D. N., & Wandelt, B. D. 2014b, Phys. Rev. D, 89, 063536
Miranda, V., & Hu, W. 2014, Phys. Rev. D, 89, 083529
Mizuno, S., & Koyama, K. 2010, Phys. Rev. D, 82, 103518
Mollerach, S. 1990, Phys. Rev. D, 42, 313
Moroi, T., & Takahashi, T. 2001, Phys. Lett. B, 522, 215
Mortonson, M. J., & Hu, W. 2008, ApJ, 672, 737
Mortonson, M. J., Dvorkin, C., Peiris, H. V., & Hu, W. 2009, Phys. Rev. D, 79, 103519
Mortonson, M. J., Peiris, H. V., & Easther, R. 2011, Phys. Rev. D, 83, 043505
Mortonson, M. J., & Seljak, U. 2014, JCAP, 1410, 035
Moss, A., Scott, D., Zibin, J. P., & Battye, R. 2011, Phys. Rev. D, 84, 023014
Mukhanov, V. 2013, Eur. Phys. J. C, 73, 2486
Mukhanov, V. F., & Chibisov, G. 1981, JETP Lett., 33, 532
Naruko, A., Komatsu, E., & Yamaguchi, M. 2015, J. Cosmol. Astropart. Phys., 2015, 45
Nicolis, A., Rattazzi, R., & Trincherini, E. 2009, Phys. Rev. D, 79, 064036
Norena, J., Wagner, C., Verde, L., Peiris, H. V., & Easther, R. 2012, Phys. Rev. D, 86, 023505
Ohashi, J., & Tsujikawa, S. 2012, JCAP, 10, 35
Ohashi, J., Soda, J., & Tsujikawa, S. 2013, Phys. Rev. D, 87, 083520
Okamoto, T., & Hu, W. 2003, Phys. Rev. D, 67, 083002
Page, L., Hinshaw, G., Komatsu, E., et al. 2007, ApJS, 170, 335
Pajer, E., & Peloso, M. 2013, Class. Quant. Grav., 30, 214002
Palanque-Delabrouille, N., Yèche, C., Lesgourgues, J., et al. 2015, J. Cosmol. Astropart. Phys., 2015, 45
Peebles, P., & Yu, J. 1970, ApJ, 162, 815
Peiris, H., & Easther, R. 2006a, JCAP, 0607, 002

Peiris, H., & Easther, R. 2006b, JCAP, 0610, 017
Peiris, H. V., & Easther, R. 2008, JCAP, 0807, 024
Peiris, H. V., Komatsu, E., Verde, L., et al. 2003, ApJS, 148, 213
Peiris, H., Baumann, D., Friedman, B., & Cooray, A. 2007, Phys. Rev. D, 76, 103517
Peiris, H., Easther, R., & Flauger, R. 2013, JCAP, 1309, 018
Perotto, L., Lesgourgues, J., Hannestad, S., Tu, H., & Wong, Y. Y. 2006, JCAP, 0610, 013
Planck Collaboration XV. 2014, A&A, 571, A15
Planck Collaboration XVI. 2014, A&A, 571, A16
Planck Collaboration XVII. 2014, A&A, 571, A17
Planck Collaboration XXII. 2014, A&A, 571, A22
Planck Collaboration XXIII. 2014, A&A, 571, A23
Planck Collaboration XXIV. 2014, A&A, 571, A24
Planck Collaboration XXV. 2014, A&A, 571, A25
Planck Collaboration XXVI. 2014, A&A, 571, A26
Planck Collaboration XXVII. 2014, A&A, 571, A27
Planck Collaboration XXX. 2014, A&A, 571, A30
Planck Collaboration XXXI. 2014, A&A, 571, A31
Planck Collaboration I. 2016, A&A, 594, A1
Planck Collaboration II. 2016, A&A, 594, A2
Planck Collaboration III. 2016, A&A, 594, A3
Planck Collaboration IV. 2016, A&A, 594, A4
Planck Collaboration V. 2016, A&A, 594, A5
Planck Collaboration VI. 2016, A&A, 594, A6
Planck Collaboration VII. 2016, A&A, 594, A7
Planck Collaboration VIII. 2016, A&A, 594, A8
Planck Collaboration IX. 2016, A&A, 594, A9
Planck Collaboration X. 2016, A&A, 594, A10
Planck Collaboration XI. 2016, A&A, 594, A11
Planck Collaboration XII. 2016, A&A, 594, A12
Planck Collaboration XIII. 2016, A&A, 594, A13
Planck Collaboration XIV. 2016, A&A, 594, A14
Planck Collaboration XV. 2016, A&A, 594, A15
Planck Collaboration XVI. 2016, A&A, 594, A16
Planck Collaboration XVII. 2016, A&A, 594, A17
Planck Collaboration XVIII. 2016, A&A, 594, A18
Planck Collaboration XIX. 2016, A&A, 594, A19
Planck Collaboration XX. 2016, A&A, 594, A20
Planck Collaboration XXI. 2016, A&A, 594, A21
Planck Collaboration XXII. 2016, A&A, 594, A22
Planck Collaboration XXIII. 2016, A&A, 594, A23
Planck Collaboration XXIV. 2016, A&A, 594, A24
Planck Collaboration XXV. 2016, A&A, 594, A25
Planck Collaboration XXVI. 2016, A&A, 594, A26
Planck Collaboration XXVII. 2016, A&A, 594, A27
Planck Collaboration XXVIII. 2016, A&A, 594, A28
Planck Collaboration Int. XIX. 2015, A&A, 576, A104
Planck Collaboration Int. XX. 2015, A&A, 576, A105
Planck Collaboration Int. XXI. 2015, A&A, 576, A106
Planck Collaboration Int. XXII. 2015, A&A, 576, A107
Planck Collaboration Int. XXX. 2016, A&A, 586, A133
Polarski, D., & Starobinsky, A. A. 1996, Class. Quant. Grav., 13, 377
Powell, B. A., & Kinney, W. H. 2007, JCAP, 0708, 006
Powell, B. A., Tzirakis, K., & Kinney, W. H. 2009, JCAP, 4, 19
Powell, M. J. D. 2009, The BoBYQA algorithm for bound constrained optimization without derivatives
Regan, D., Anderson, G. J., Hull, M., & Seery, D. 2015, J. Cosmol. Astropart. Phys., 2015, 15
Ross, A. J., Samushia, L., Howlett, C., et al. 2015, MNRAS., 449, 835
Rossi, G., Yeche, C., Palanque-Delabrouille, N., & Lesgourgues, J. 2015, Phys. Rev. D, 92, 063505
Sasaki, M., Valiviita, J., & Wands, D. 2006, Phys. Rev. D, 74, 103003
Savelainen, M., Valiviita, J., Walia, P., Rusak, S., & Kurki-Suonio, H. 2013, Phys. Rev. D, 88, 063010
Schmidt, F., & Hui, L. 2013, Phys. Rev. Lett., 110, 011301
Seljak, U., & Zaldarriaga, M. 1997, Phys. Rev. Lett., 78, 2054
Senatore, L., Smith, K. M., & Zaldarriaga, M. 2010, JCAP, 1, 28
Silverstein, E., & Tong, D. 2004, Phys. Rev. D, 70, 103505
Silverstein, E., & Westphal, A. 2008, Phys. Rev. D, 78, 106003
Soda, J. 2012, Class. Quant. Grav., 29, 083001
Sorbo, L. 2011, JCAP, 6, 3
Starobinsky, A. 1983, Sov. Astron. Lett., 9, 302
Starobinsky, A. A. 1980, Phys. Lett. B, 91, 99
Starobinsky, A. A. 1992, JETP Lett., 55, 489
Stewart, A., & Brandenberger, R. 2008, JCAP, 0808, 012
Stewart, E. D. 1995, Phys. Rev. D, 51, 6847
Stewart, E. D., & Lyth, D. H. 1993, Phys. Lett. B, 302, 171
Tsujikawa, S. 2014, PTEP, 2014, 06B104
Tsujikawa, S., Ohashi, J., Kuroyanagi, S., & De Felice, A. 2013, Phys. Rev. D, 88, 023529
Turner, M. S. 1983, Phys. Rev. D, 28, 1243
Unnikrishnan, S., Sahni, V., & Toporensky, A. 2012, JCAP, 1208, 018
Valiviita, J., & Giannantonio, T. 2009, Phys. Rev. D, 80, 123516
Valiviita, J., Savelainen, M., Talvitie, M., Kurki-Suonio, H., & Rusak, S. 2012, ApJ, 753, 151
Vázquez, J. A., Bridges, M., Hobson, M. P., & Lasenby, A. N. 2012, JCAP, 6, 6
Vilenkin, A. 1985, Phys. Rev. D, 32, 2511
Wands, D., Bartolo, N., Matarrese, S., & Riotto, A. 2002, Phys. Rev. D, 66, 043520
Weinberg, S. 2004, Phys. Rev. D, 70, 083522
White, M., Scott, D., & Silk, J. 1994, Ann. Rev. Ast. Astro, 32, 319
Zaldarriaga, M., & Seljak, U. 1997, Phys. Rev. D, 55, 1830
Zeldovich, Y. 1972, MNRAS, 160, 1P

[1] APC, AstroParticule et Cosmologie, Université Paris Diderot, CNRS/IN2P3, CEA/lrfu, Observatoire de Paris, Sorbonne Paris Cité, 10 rue Alice Domon et Léonie Duquet, 75205 Paris Cedex 13, France
[2] Aalto University Metsähovi Radio Observatory and Dept of Radio Science and Engineering, PO Box 13000, 00076 Aalto, Finland
[3] African Institute for Mathematical Sciences, 6−8 Melrose Road, Muizenberg, 7945 Cape Town, South Africa
[4] Agenzia Spaziale Italiana Science Data Center, via del Politecnico snc, 00133 Roma, Italy
[5] Aix-Marseille Université, CNRS, LAM (Laboratoire d'Astrophysique de Marseille) UMR 7326, 13388 Marseille, France
[6] Astrophysics Group, Cavendish Laboratory, University of Cambridge, J J Thomson Avenue, Cambridge CB3 0HE, UK
[7] Astrophysics & Cosmology Research Unit, School of Mathematics, Statistics & Computer Science, University of KwaZulu-Natal, Westville Campus, Private Bag X54001, 4000 Durban, South Africa
[8] Atacama Large Millimeter/submillimeter Array, ALMA Santiago Central Offices, Alonso de Cordova 3107, Vitacura, 763 0355 Casilla, Santiago, Chile
[9] CGEE, SCS Qd 9, Lote C, Torre C, 4° andar, Ed. Parque Cidade Corporate, CEP 70308-200 Brasília, DF, Brazil
[10] CITA, University of Toronto, 60 St. George St., Toronto, ON M5S 3H8, Canada
[11] CNRS, IRAP, 9 Av. colonel Roche, BP 44346, 31028 Toulouse Cedex 4, France
[12] CRANN, Trinity College, Dublin 2, Ireland
[13] California Institute of Technology, Pasadena, CA 91125, USA
[14] Centre for Theoretical Cosmology, DAMTP, University of Cambridge, Wilberforce Road, Cambridge CB3 0WA, UK
[15] Centro de Estudios de Física del Cosmos de Aragón (CEFCA), Plaza San Juan, 1, planta 2, 44001 Teruel, Spain
[16] Computational Cosmology Center, Lawrence Berkeley National Laboratory, Berkeley, CA 94720, USA
[17] Consejo Superior de Investigaciones Científicas (CSIC), 28049 Madrid, Spain
[18] DSM/Irfu/SPP, CEA-Saclay, 91191 Gif-sur-Yvette Cedex, France
[19] DTU Space, National Space Institute, Technical University of Denmark, Elektrovej 327, 2800 Kgs. Lyngby, Denmark
[20] Département de Physique Théorique, Université de Genève, 24 quai E. Ansermet, 1211 Genève 4, Switzerland
[21] Dark Cosmology Centre, Niels Bohr Institute, University of Copenhagen, Juliane Maries Vej 30, 2100 Copenhagen, Denmark
[22] Departamento de Astrofísica, Universidad de La Laguna (ULL), 38206 La Laguna, Tenerife, Spain
[23] Departamento de Física, Universidad de Oviedo, Avda. Calvo Sotelo s/n, 33007 Oviedo, Spain
[24] Department of Astronomy and Astrophysics, University of Toronto, 50 Saint George Street, Toronto, Ontario, ON M5S 3H41, Canada
[25] Department of Astrophysics/IMAPP, Radboud University Nijmegen, PO Box 9010, 6500 GL Nijmegen, The Netherlands

[26] Department of Physics & Astronomy, University of British Columbia, 6224 Agricultural Road, Vancouver, British Columbia, Canada
[27] Department of Physics and Astronomy, Dana and David Dornsife College of Letter, Arts and Sciences, University of Southern California, Los Angeles, CA 90089, USA
[28] Department of Physics and Astronomy, University College London, London WC1E 6BT, UK
[29] Department of Physics and Astronomy, University of Sussex, Brighton BN1 9QH, UK
[30] Department of Physics, Florida State University, Keen Physics Building, 77 Chieftan Way, Tallahassee, Florida, USA
[31] Department of Physics, Gustaf Hällströmin katu 2a, University of Helsinki, 00560 Helsinki, Finland
[32] Department of Physics, Princeton University, Princeton, NJ 08540, USA
[33] Department of Physics, University of California, Berkeley, CA 94720, USA
[34] Department of Physics, University of California, Santa Barbara, California, USA
[35] Department of Physics, University of Illinois at Urbana-Champaign, 1110 West Green Street, Urbana, Illinois, USA
[36] Dipartimento di Fisica e Astronomia G. Galilei, Università degli Studi di Padova, via Marzolo 8, 35131 Padova, Italy
[37] Dipartimento di Fisica e Astronomia, ALMA MATER STUDIORUM, Università degli Studi di Bologna, viale Berti Pichat 6/2, 40127 Bologna, Italy
[38] Dipartimento di Fisica e Scienze della Terra, Università di Ferrara, via Saragat 1, 44122 Ferrara, Italy
[39] Dipartimento di Fisica, Università La Sapienza, P.le A. Moro 2, 00133 Roma, Italy
[40] Dipartimento di Fisica, Università degli Studi di Milano, via Celoria, 16, 00133 Milano, Italy
[41] Dipartimento di Fisica, Università degli Studi di Trieste, via A. Valerio 2, 00133 Trieste, Italy
[42] Dipartimento di Matematica, Università di Roma Tor Vergata, via della Ricerca Scientifica, 1, 00133 Roma, Italy
[43] Discovery Center, Niels Bohr Institute, Blegdamsvej 17, 1165 Copenhagen, Denmark
[44] Discovery Center, Niels Bohr Institute, Copenhagen University, Blegdamsvej 17, 1165 Copenhagen, Denmark
[45] European Southern Observatory, ESO Vitacura, Alonso de Cordova 3107, Vitacura, Casilla 19001, Santiago, Chile
[46] European Space Agency, ESAC, Planck Science Office, Camino bajo del Castillo, s/n, Urbanización Villafranca del Castillo, 28691 Villanueva de la Cañada, Madrid, Spain
[47] European Space Agency, ESTEC, Keplerlaan 1, 2201 AZ Noordwijk, The Netherlands
[48] Gran Sasso Science Institute, INFN, viale F. Crispi 7, 67100 L'Aquila, Italy
[49] HGSFP and University of Heidelberg, Theoretical Physics Department, Philosophenweg 16, 69120 Heidelberg, Germany
[50] Helsinki Institute of Physics, Gustaf Hällströmin katu 2, University of Helsinki, 00560 Helsinki, Finland
[51] INAF–Osservatorio Astronomico di Padova, Vicolo dell'Osservatorio 5, 35131 Padova, Italy
[52] INAF–Osservatorio Astronomico di Roma, via di Frascati 33, 00040 Monte Porzio Catone, Italy
[53] INAF–Osservatorio Astronomico di Trieste, via G.B. Tiepolo 11, 34127 Trieste, Italy
[54] INAF/IASF Bologna, via Gobetti 101, 40127 Bologna, Italy
[55] INAF/IASF Milano, via E. Bassini 15, 20133 Milano, Italy
[56] INFN, Sezione di Bologna, via Irnerio 46, 40126 Bologna, Italy
[57] INFN, Sezione di Roma 1, Università di Roma Sapienza, P.le Aldo Moro 2, 00185 Roma, Italy
[58] INFN, Sezione di Roma 2, Università di Roma Tor Vergata, via della Ricerca Scientifica, 1, 00185 Roma, Italy
[59] INFN/National Institute for Nuclear Physics, via Valerio 2, 34127 Trieste, Italy
[60] IPAG: Institut de Planétologie et d'Astrophysique de Grenoble, Université Grenoble Alpes, IPAG, 38000 Grenoble, France; CNRS, IPAG, 38000 Grenoble, France
[61] IUCAA, Post Bag 4, Ganeshkhind, Pune University Campus, 411 007 Pune, India
[62] Imperial College London, Astrophysics group, Blackett Laboratory, Prince Consort Road, London, SW7 2AZ, UK
[63] Infrared Processing and Analysis Center, California Institute of Technology, Pasadena, CA 91125, USA
[64] Institut Néel, CNRS, Université Joseph Fourier Grenoble I, 25 rue des Martyrs, 38042 Grenoble, France
[65] Institut Universitaire de France, 103 bd Saint-Michel, 75005 Paris, France
[66] Institut d'Astrophysique Spatiale, CNRS, Univ. Paris-Sud, Université Paris-Saclay, Bât. 121, 91405 Orsay Cedex, France
[67] Institut d'Astrophysique de Paris, CNRS (UMR 7095), 98bis boulevard Arago, 75014 Paris, France
[68] Institut für Theoretische Teilchenphysik und Kosmologie, RWTH Aachen University, 52056 Aachen, Germany
[69] Institute for Space Sciences, Bucharest-Magurale, Romania
[70] Institute of Astronomy, University of Cambridge, Madingley Road, Cambridge CB3 0HA, UK
[71] Institute of Theoretical Astrophysics, University of Oslo, Blindern, 0371 Oslo, Norway
[72] Instituto de Astrofísica de Canarias, C/Vía Láctea s/n, 28205 La Laguna, Tenerife, Spain
[73] Instituto de Física de Cantabria (CSIC-Universidad de Cantabria), Avda. de los Castros s/n, 39005 Santander, Spain
[74] Istituto Nazionale di Fisica Nucleare, Sezione di Padova, via Marzolo 8, 35131 Padova, Italy
[75] Jet Propulsion Laboratory, California Institute of Technology, 4800 Oak Grove Drive, Pasadena, California, USA
[76] Jodrell Bank Centre for Astrophysics, Alan Turing Building, School of Physics and Astronomy, The University of Manchester, Oxford Road, Manchester, M13 9PL, UK
[77] Kavli Institute for Cosmological Physics, University of Chicago, Chicago, IL 60637, USA
[78] Kavli Institute for Cosmology Cambridge, Madingley Road, Cambridge, CB3 0HA, UK
[79] Kazan Federal University, 18 Kremlyovskaya St., 420008 Kazan, Russia
[80] LAL, Université Paris-Sud, CNRS/IN2P3, Orsay, France
[81] LERMA, CNRS, Observatoire de Paris, 61 avenue de l'Observatoire, 75000 Paris, France
[82] Laboratoire AIM, IRFU/Service d'Astrophysique – CEA/DSM – CNRS – Université Paris Diderot, Bât. 709, CEA-Saclay, 91191 Gif-sur-Yvette Cedex, France
[83] Laboratoire Traitement et Communication de l'Information, CNRS (UMR 5141) and Télécom ParisTech, 46 rue Barrault 75634 Paris Cedex 13, France
[84] Laboratoire de Physique Subatomique et Cosmologie, Université Grenoble-Alpes, CNRS/IN2P3, 53 rue des Martyrs, 38026 Grenoble Cedex, France
[85] Laboratoire de Physique Théorique, Université Paris-Sud 11 & CNRS, Bâtiment 210, 91405 Orsay, France
[86] Lawrence Berkeley National Laboratory, Berkeley, California, USA
[87] Lebedev Physical Institute of the Russian Academy of Sciences, Astro Space Centre, 84/32 Profsoyuznaya st., 117997 Moscow, GSP-7, Russia
[88] Leung Center for Cosmology and Particle Astrophysics, National Taiwan University, 10617 Taipei, Taiwan
[89] Max-Planck-Institut für Astrophysik, Karl-Schwarzschild-Str. 1, 85741 Garching, Germany
[90] McGill Physics, Ernest Rutherford Physics Building, McGill University, 3600 rue University, Montréal, QC, H3A 2T8, Canada
[91] National University of Ireland, Department of Experimental Physics, Maynooth, Co. Kildare, Ireland
[92] Nicolaus Copernicus Astronomical Center, Bartycka 18, 00-716 Warsaw, Poland

[93] Niels Bohr Institute, Blegdamsvej 17, 1165 Copenhagen, Denmark
[94] Niels Bohr Institute, Copenhagen University, Blegdamsvej 17, 1165 Copenhagen, Denmark
[95] Nordita (Nordic Institute for Theoretical Physics), Roslagstullsbacken 23, 106 91 Stockholm, Sweden
[96] Optical Science Laboratory, University College London, Gower Street, London, UK
[97] SISSA, Astrophysics Sector, via Bonomea 265, 34136 Trieste, Italy
[98] SMARTEST Research Centre, Università degli Studi e-Campus, via Isimbardi 10, 22060 Novedrate (CO), Italy
[99] School of Physics and Astronomy, Cardiff University, Queens Buildings, The Parade, Cardiff, CF24 3AA, UK
[100] School of Physics and Astronomy, University of Nottingham, Nottingham NG7 2RD, UK
[101] Simon Fraser University, Department of Physics, 8888 University Drive, Burnaby BC, Canada
[102] Sorbonne Université-UPMC, UMR 7095, Institut d'Astrophysique de Paris, 98bis boulevard Arago, 75014 Paris, France
[103] Space Research Institute (IKI), Russian Academy of Sciences, Profsoyuznaya Str, 84/32, 117997 Moscow, Russia
[104] Space Sciences Laboratory, University of California, Berkeley, CA 94720, USA
[105] Special Astrophysical Observatory, Russian Academy of Sciences, Nizhnij Arkhyz, Zelenchukskiy region, 369167 Karachai-Cherkessian Republic, Russia
[106] Stanford University, Dept of Physics, Varian Physics Bldg, 382 via Pueblo Mall, Stanford, California, USA
[107] Sub-Department of Astrophysics, University of Oxford, Keble Road, Oxford OX1 3RH, UK
[108] Sydney Institute for Astronomy, School of Physics A28, University of Sydney, NSW 2006, Australia
[109] The Oskar Klein Centre for Cosmoparticle Physics, Department of Physics,Stockholm University, AlbaNova, 106 91 Stockholm, Sweden
[110] Theory Division, PH-TH, CERN, 1211 Geneva 23, Switzerland
[111] UPMC Univ Paris 06, UMR7095, 98bis boulevard Arago, 75014 Paris, France
[112] Université de Toulouse, UPS-OMP, IRAP, 31028 Toulouse Cedex 4, France
[113] Universities Space Research Association, Stratospheric Observatory for Infrared Astronomy, MS 232-11, Moffett Field, CA 94035, USA
[114] University of Granada, Departamento de Física Teórica y del Cosmos, Facultad de Ciencias, 18071 Granada, Spain
[115] University of Granada, Instituto Carlos I de Física Teórica y Computacional, 18071 Granada, Spain
[116] Warsaw University Observatory, Aleje Ujazdowskie 4, 00-478 Warszawa, Poland